



**HAL**  
open science

# The predictive capacity of the MADYMO ellipsoid pedestrian model for pedestrian ground contact kinematics and injury evaluation

Shi Shang, Catherine Masson, Maxime Llari, Max Py, Quentin Ferrand, Pierre-Jean Arnoux, Ciaran Simms

## ► To cite this version:

Shi Shang, Catherine Masson, Maxime Llari, Max Py, Quentin Ferrand, et al.. The predictive capacity of the MADYMO ellipsoid pedestrian model for pedestrian ground contact kinematics and injury evaluation. *Accident Analysis & Prevention*, 2021, 149, pp.105803. 10.1016/j.aap.2020.105803 . hal-04082952

**HAL Id: hal-04082952**

**<https://amu.hal.science/hal-04082952v1>**

Submitted on 27 Apr 2023

**HAL** is a multi-disciplinary open access archive for the deposit and dissemination of scientific research documents, whether they are published or not. The documents may come from teaching and research institutions in France or abroad, or from public or private research centers.

L'archive ouverte pluridisciplinaire **HAL**, est destinée au dépôt et à la diffusion de documents scientifiques de niveau recherche, publiés ou non, émanant des établissements d'enseignement et de recherche français ou étrangers, des laboratoires publics ou privés.



Distributed under a Creative Commons Attribution 4.0 International License

1 **The predictive capacity of the MADYMO ellipsoid pedestrian model**  
2 **for pedestrian ground contact injury evaluation**

3  
4 Shi Shang<sup>1</sup>, Catherine Masson<sup>2</sup>, Maxime Llari<sup>2</sup>, Max Py<sup>2</sup>, Quentin Ferrand<sup>2</sup>, Pierre-Jean Arnoux<sup>2</sup>, Ciaran  
5 Simms<sup>1</sup>

6 <sup>1</sup>Trinity Centre for Bioengineering, Trinity College Dublin, Ireland

7 <sup>2</sup>Laboratoire de Biomécanique Appliquée (IFSTTAR – Université de la Méditerranée), France

8  
9 Email: ([sshang@tcd.ie](mailto:sshang@tcd.ie))

10  
11 ***Abstract***

12 Pedestrian injuries occur in both the primary vehicle contact and the subsequent ground contact.  
13 Currently, no ground contact countermeasures have been implemented and no pedestrian model has  
14 been validated for ground contact, though this is needed for developing future ground contact injury  
15 countermeasures. In this paper, we assess the predictive capacity of the MADYMO pedestrian model  
16 in reconstructing six recent pedestrian cadaver ground contact experiments. Whole-body kinematics  
17 as well as vehicle and ground contact related *HIC* and *BrIC* scores were evaluated. Reasonable  
18 results were generally achieved for the timings of the principal collision events, and for the overall  
19 ground contact mechanisms. However, the resulting head injury predictions based on the ground  
20 contact *HIC* and *BrIC* scores showed limited capacity of the model to replicate individual  
21 experiments. Sensitivity studies showed substantial influences of the vehicle- pedestrian contact  
22 characteristic and certain initial pedestrian joint angles on the subsequent ground contact injury  
23 predictions. Further work is needed to improve the predictive capacity of the MADYMO pedestrian  
24 model for ground contact injury predictions.

25  
26  
27 ***Keywords***

28 Pedestrians, vehicle contact, ground contact, MADYMO model assessment  
29  
30

31 **1. Introduction**

32 The World Health Organization (WHO) estimates that more than 300,000 pedestrians have died in  
33 2019 (WHO 2020), based on its Global Status Report on Road Safety 2018 (WHO 2018). Pedestrian  
34 collisions usually involve a primary contact with the vehicle, followed by a secondary contact with  
35 the ground (Han *et al.* 2018, Shang 2020). Accordingly, although most research has focused on  
36 vehicle contact (Kerrigan *et al.* 2007, Yao *et al.* 2008), the significance of the ground contact has also  
37 been emphasized (Simms and Wood 2006, Crocetta *et al.* 2015, Han *et al.* 2018, Shang *et al.* 2018,  
38 Shi *et al.* 2019, Shang *et al.* 2020b). A recent analysis based on German real-world crash data  
39 (GIDAS) showed that 43% of 1221 selected cases had injuries subjected to ground contact,  
40 demonstrating the importance of ground related pedestrian injuries and providing significant  
41 motivation for countermeasures to prevent or moderate pedestrian injuries from ground contact  
42 (Shang *et al.* 2018). (Shang *et al.* 2020b) recently conducted six cadaver tests which recorded the  
43 whole process from vehicle contact until after the end of the ground contact. They observed that peak  
44 linear accelerations in ground contact are generally higher than for the vehicle contact. They also  
45 observed a high predicted risk of rotationally induced brain injury from ground contact, even for very  
46 low vehicle collision speeds.

47 However, many open questions remain regarding the influence of vehicle front shape and the design  
48 of potential countermeasures to minimize pedestrian ground contact injuries, and a suitably validated  
49 computational model is a much more sustainable tool for addressing these than cadaver experiments.

50 The MADYMO 50<sup>th</sup> percentile male pedestrian model, developed by TNO Automotive, is the  
51 most commonly used multibody pedestrian models for vulnerable road user crash reconstruction (van  
52 Hoof *et al.* 2003, van Rooij *et al.* 2003, Simms and Wood 2006, Untaroiu *et al.* 2009, Elliott *et al.*  
53 2012, Xu *et al.* 2016, Shang *et al.* 2018). The model was validated for both full model (Ishikawa *et al.*  
54 1993) and model segments such as tibia and femur static 3-point bending tests, cadaver side  
55 impact tests for the pelvis, thorax and shoulder, cadaver leg impactor tests for bending moment and  
56 shear force of lower extremities (Kajzer *et al.* 1993). De Lange *et al.* (DeLange *et al.* 2006) verified  
57 the kinematics of the MADYMO pedestrian model with eighteen full vehicle-pedestrian impact tests.  
58 However, the validation was only for vehicle contact and not for ground contact, even though it has  
59 since been applied for analyzing the ground contact (Crocetta *et al.* 2015, Zou *et al.* 2019). (Crocetta  
60 *et al.* 2015) defined six different pedestrian ground impact mechanisms by simulating hundreds of

61 impact configurations with different vehicle shapes, pedestrian heights and vehicle speeds, with  
62 partial validation by comparison to real-world videos (Barry and Simms 2016). The model has also  
63 been applied in the use of potential braking related countermeasures (Zou *et al.* 2019). However, the  
64 capacity of the MADYMO pedestrian model to replicate kinematics of individual pedestrian ground  
65 contact collisions remains unknown.

66

67 Researchers also developed other multibody or finite element pedestrian models for vehicle-  
68 pedestrian collisions. (Yang and Lovsund 1997) developed a 3D MB pedestrian model with emphasis  
69 on the head and lower extremities. The model consists of fifteen body segments with fourteen joints.  
70 The leg segments are breakable (Yang *et al.* 1993) and the knee joint formulation (Yang *et al.* 1995)  
71 facilitates biofidelic responses of the knees and leg fracture. The model was validated based on  
72 pedestrian substitutes' kinematics, the body segments' accelerations, contact forces, and failure  
73 descriptions compared with previously published cadaver impacts (Ishikawa *et al.* 1993). Finite  
74 element pedestrian models such as THUMS (Maeno and Hasegawa 2001, Iwamoto *et al.* 2003) and  
75 GHBMC (Untaroiu *et al.* 2016) pedestrian models are developed to simulate deformable vehicle-  
76 pedestrian impact scenarios. However, none of these models have been validated for ground contact.

77

78 In summary, a variety of pedestrian models (multibody and finite element) have been developed and  
79 applied to vulnerable road user crashes. These have been validated based on lower extremity bending  
80 and shear loadings, the head response including acceleration and force, head trajectories, whole-body  
81 kinematics etc. However, all models are validated for the vehicle impact only, and model validations  
82 for ground contact are so far lacking. The importance of pedestrian ground contact is growing and  
83 the risk of suffering serious head brain injury due to ground contact has been recently highlighted  
84 (Shang *et al.* 2018, Shang *et al.* 2020b). Given the high cost of cadaver tests, there is significant  
85 value in a pedestrian model which can simulate the ground impact and can be applied in large-  
86 sample parametric study such as virtual test system (Li *et al.* 2018). The recent staged cadaver  
87 impact tests (Shang *et al.* 2020b) provide a valuable experimental reference set, including pedestrian  
88 kinematics and injury criteria evaluations (skull fracture, *HIC* and *BrIC*) for multi-body model  
89 assessment.

90 Accordingly, the aims of the current study are to:

- 91 1) reconstruct the cadaver impact tests of (Shang *et al.* 2020b) to assess the capability of the  
92 MADYMO pedestrian model for use in ground contact scenarios, and assess the  
93 difference between the MADYMO multibody model and the cadaver in post-impact  
94 kinematics and head injury criteria predictions.
- 95 2) Perform sensitivity studies to assess the influence of the vehicle pedestrian contact  
96 characteristics, the influence of initial pedestrian position on subsequent pedestrian  
97 ground contact and the effect of internal damping on overall body kinematics.

98 If the pedestrian model can reasonably replicate kinematics and injury outcomes, it may be suitable  
99 for investigating the effect of vehicle front shape on the risk of pedestrian ground contact injuries  
100 over a broad range of collision configurations. Moreover, it could be used for developing active  
101 countermeasures to prevent pedestrian ground contact related injuries, such as controlled braking or  
102 airbag technologies (Khaykin and Larner 2016, Zou *et al.* 2019).

## 104 **2. *Materials and methods***

105 The MADYMO ellipsoid multibody pedestrian model, as well as simplified vehicle models, were  
106 employed to assess their performance in ground contact, by comparison with the cadaver tests  
107 reported in (Shang *et al.* 2020b), see Figure 1.

108  
109 Given uncertainty in several input characteristics of the models, sensitivity studies were designed to  
110 assess the influence of the vehicle to pedestrian contact definition (loading and unloading functions,  
111 hysteresis), internal damping in the pedestrian models and the initial pedestrian joint angles.

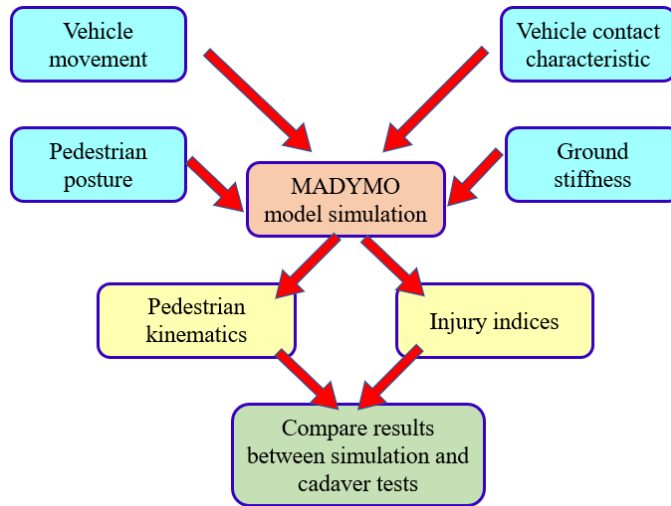


Figure 1: Steps followed in assessing the multibody models

113

### 2.1. Multibody vehicle models

114

115 Simplified multibody vehicle models were built in MADYMO, with the geometry based on (The-  
 116 Blueprints) to represent the vehicles tested in (Shang *et al.* 2020b). Each vehicle model consists of a  
 117 lower bumper, bumper, bonnet leading edge, bonnet, windshield, wheels and roof, see Figure 2.

118

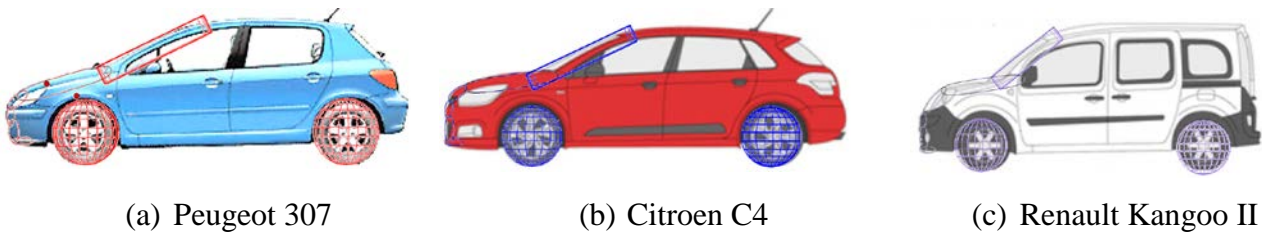


Figure 2 The vehicle models with the simplified MADYMO models

119

### 2.2. Pedestrian models

120

121 The heights and weights of the pedestrian cadavers varied, as shown in Table 1 of (Shang *et al.*  
 122 2020b), replicated here as Appendix A and these were replicated by scaling the MADYMO 50<sup>th</sup>  
 123 percentile pedestrian model using a customized Matlab code based on the pedestrian's height and  
 124 weight. This global scaling does not address relative differences in body segment proportions. The  
 125 scaled multibody models, as well as the corresponding pedestrian cadavers are shown in Figure 3.  
 126 The initial postures (joint angles) of the models were adjusted based on the measurements of cadaver  
 127 poses from the side and the front views which were captured pre-impact. Due to the joint limitation  
 128 of the pedestrian model and the segment dimension differences, some differences between cadaver

129 and the simulation postures exist, see for example the left forearm in Figure 3 (a). For Test 05 in  
130 Figure 3 (e), the posture is the result of difficulties with initial placement of the cadaver which had  
131 very low mass (38kg) and unusually stiff joints (the cause of this is unknown as full medical histories  
132 were not available).  
133

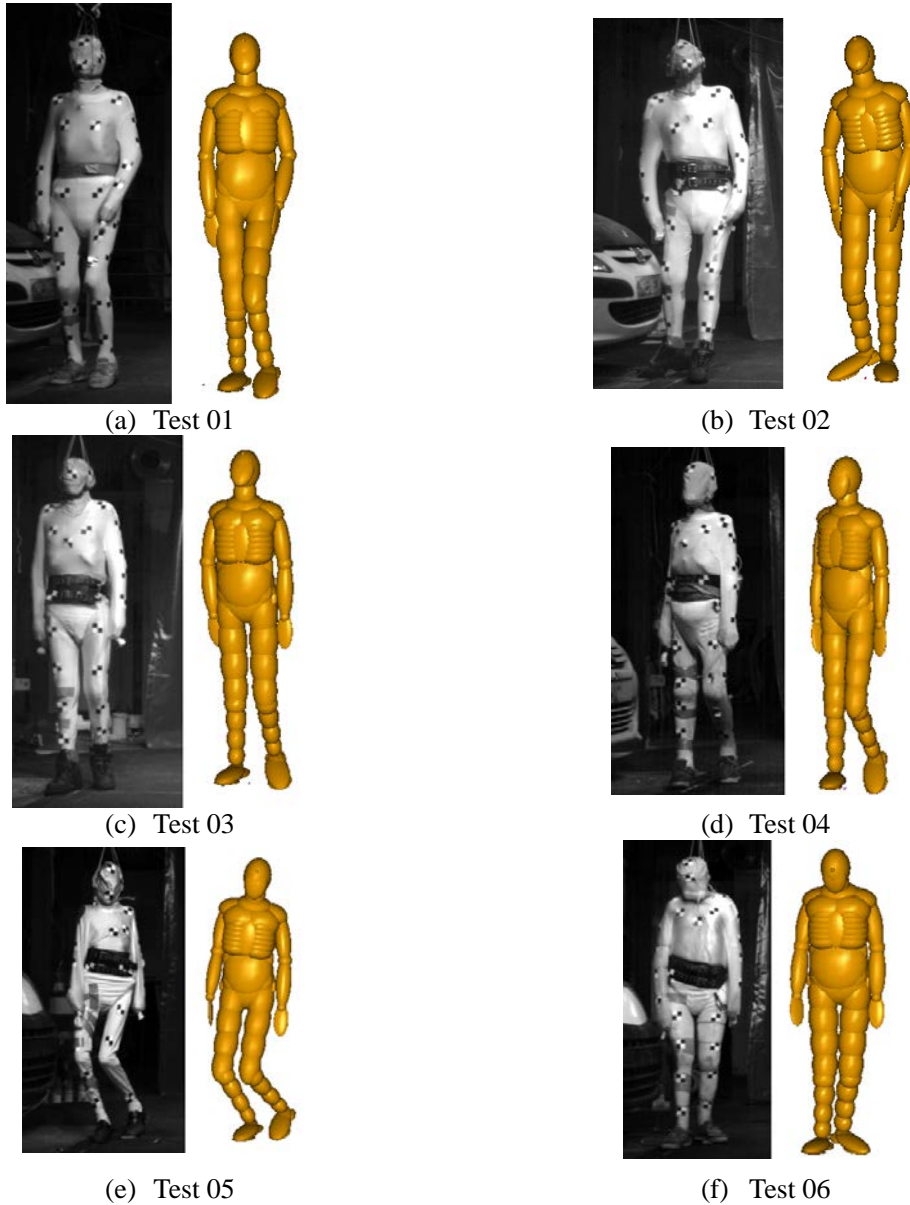


Figure 3 The initial postures of PMHS pedestrians and the corresponding scaled multi-body models

### 134 2.3. Movement input of the multibody vehicle models

135 The planar time-displacement curves in the X (horizontal) direction and the Z (vertical) direction,  
136 and the time-rotation curve of the vehicle, were extracted every 20ms (overall impact duration was  
137 approximately one second) using a customized Matlab script and used to prescribe the vehicle

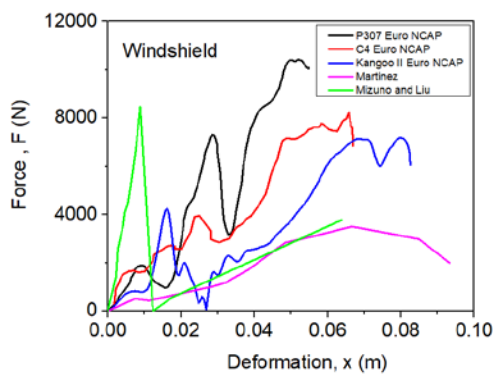
138 motion in the models. The general steps for selecting the tracking points are as shown in Appendix  
139 B.

140

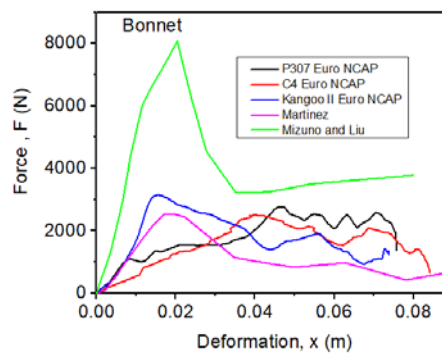
#### 141 2.4. Contact characteristic applied on the MB vehicle model

142 Three sources of vehicle contact characteristic were available: the published force-deformation  
143 characteristics derived from impactor tests (Martinez *et al.* 2007), recent test on the actual vehicle  
144 types performed by the European New Car Assessment Programme (EURO-NCAP) (Euro-NCAP)  
145 and another older force deformation characteristics from impactor tests (Mizuno and Kajzer 2000)  
146 and (Liu *et al.* 2002). The windshield and bonnet stiffness from (Mizuno and Kajzer 2000) were  
147 obtained by impactor tests and the stiffness of bonnet leading edge and bumper were obtained from  
148 leg form tests by (Liu *et al.* 2002). This combination of vehicle contact characteristic has previously  
149 been used by (Li *et al.* 2016) for a virtual test system. Euro NCAP assesses the pedestrian safety  
150 performance of new cars with a rating (up to 5-star) based on sub-system impactor tests (Hobbs and  
151 McDonough 1998, Euro-NCAP 2010). (Martinez *et al.* 2007) summarized 425 Euro NCAP tests and  
152 then estimated a series of simplified average stiffness curves. The force-deformation curves of each  
153 tested vehicle from the Euro NCAP tests as well as the force-deformation curves from (Martinez *et*  
154 *al.* 2007) and (Mizuno and Kajzer 2000) are shown in Figure 4. The detailed process of obtaining the  
155 vehicle front stiffness by using subsystem impactors can be found in (Martinez *et al.* 2007).

156



(a) windshield



(b) bonnet



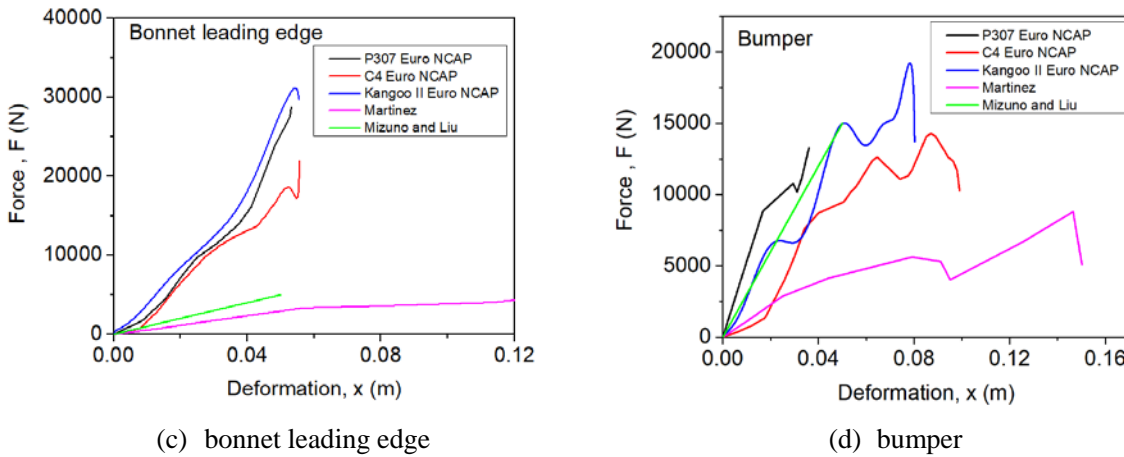


Figure 4 Force-deformation contact characteristics of vehicle front components from different sources

157

158 **2.5. Ground contact stiffness**

159 Considering the individual differences of the tested cadavers and also the different locations on the  
 160 head (some of the head contacts occurred to the face while others occurred to the posterior of the  
 161 head), the ground contact stiffness was set individually in MADYMO for each reconstruction. To  
 162 estimate the contact stiffness, a multibody sphere with inertia properties matching the head and  
 163 initial linear and angular velocities matching the experimental head kinematics just prior to head  
 164 ground contact was used to simulate the head impacts with the ground, see Table 1. The method used  
 165 to estimate the contact stiffness of the ground was based on the assumption that a quarter wave of  
 166 simple harmonic motion (Triana and Fajardo 2013) reasonably models head acceleration until the  
 167 peak is reached in the head ground impact, see Equation 1. From this, stiffness is calculated based on  
 168 the peak acceleration and speed change.

169

Table 1 The input parameter of the multibody sphere (simplified head model)

Parameter	Input
Head Mass	4.5kg
Inertia	(2.08e-02 2.37e-02 1.53e-02 0 0 0) kg·m <sup>2</sup> (directly from MADYMO 50 <sup>th</sup> percentile pedestrian model)
Linear speed	From (Shang <i>et al.</i> 2020b)
Angular speed	From (Shang <i>et al.</i> 2020b)
Initial position	0.02m high from the ground in vertical direction

170

171

172

$$\sqrt{\frac{m}{K}} = \omega = \frac{1}{\Delta T} = \frac{1}{\left(\frac{\Delta V}{Acc_{peak}}\right)} = \frac{Acc_{peak}}{\Delta V}$$

$$K = m \times \left(\frac{\Delta V}{Acc_{peak}}\right)^2$$

Equation 1

173

174 where  $m$  is the mass of the head,  $\omega$  is the natural frequency,  $\Delta T$  is the time duration of the impact,   
 175  $\Delta V$  is the speed change during impact and  $Acc_{peak}$  is the peak acceleration. The stiffness ( $K$ )   
 176 calculated for each test and the anterior/posterior head contact location are shown in Figure 5. The   
 177 head ground contact characteristics for Test 06 is not listed as the acceleration measurement was   
 178 corrupted during ground contact. As the input of Test 06 was similar to Test 05 and the pedestrian   
 179 ground contact mechanisms of the two tests were same, the stiffness of the ground for Test 06 was   
 180 set as same as that of Test 05. The comparison of the accelerations obtained from the simplified head   
 181 model with each corresponding cadaver tests are illustrated in Figure 6, and the average values were   
 182 applied for posterior and anterior head contacts. The average value of  $K$  from Test 01, Test 02 and   
 183 Test 05 was used to define  $K_p$  (posterior), as shown in Table 2, for the 30 kph tests, which have a   
 184 relatively high ground stiffness due to the posterior head impact. In contrast, in Test 03 and Test 04,   
 185 the front softer part of the head, such as the nose and face impacted the ground first, namely the   
 186 anterior head impact, and the ground contact stiffness in these two tests was set as  $K_a$  (anterior) as   
 187 shown in Table 2, using the average value of  $K$  from the corresponding tests.  $K_p$  and  $K_a$  were then   
 188 chosen as head ground contact characteristic depending on which area of the head impacts the   
 189 ground first, as determined in a pre-simulation.

190

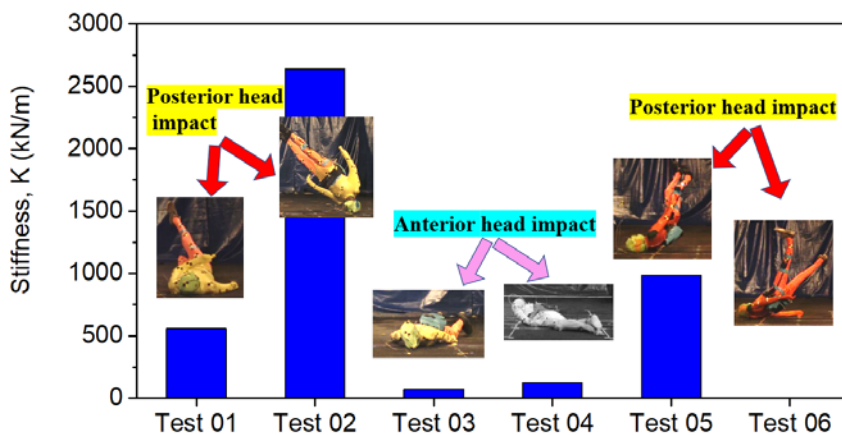
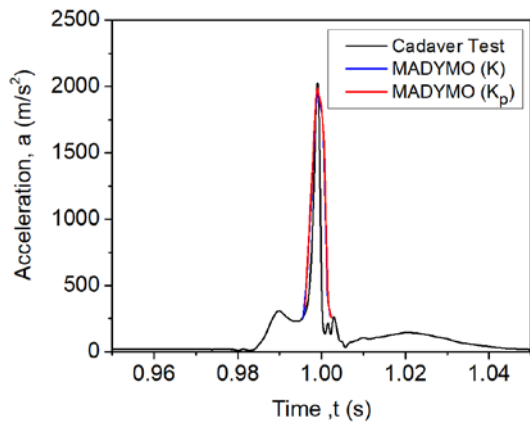
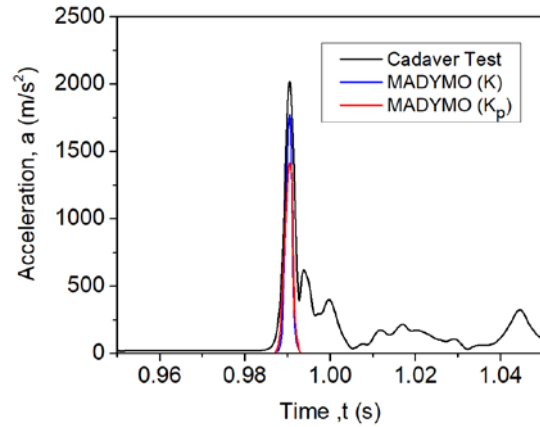


Figure 5 Ground stiffness for each test calculated

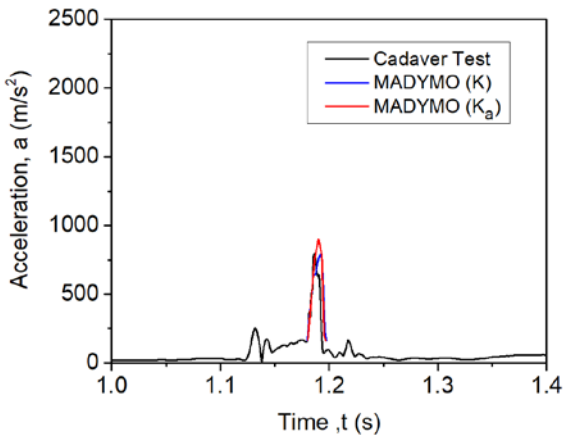
191  
192



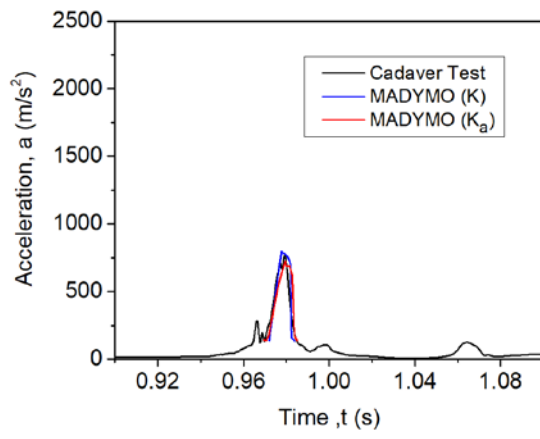
(a) Test 01



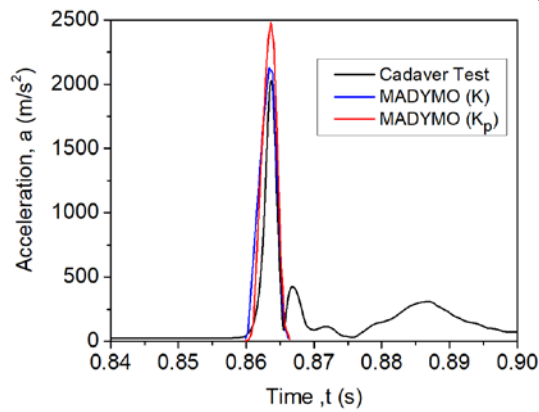
(b) Test 02



(c) Test 03



(d) Test 04



(e) Test 05

Figure 6 Comparison of the accelerations obtained from simplified head model test by using K and  $K_a$  or  $K_p$  (the comparison of Test 06 was not given because the experimental head acceleration was corrupted)

193  
194  
195  
196

197  
198

Table 2 Stiffness of ground applied in MADYMO simulations

	Value	Test used for reconstruction
$k_p$	1400 kN/m	Test 01, Test 02, Test 05 and Test 06
$k_a$	97 kN/m	Test 03 and Test 04

199

## 200 **2.6 Injury Assessments**

201 Assessments of head injury caused by translational accelerations were approximated using the *HIC*  
202 criterion, whereas injuries caused by rotational angular velocities were approximated using the *BrIC*  
203 criterion. It is noted this is not the actual *HIC* as it was not possible to fix the accelerometer to head  
204 CG in the cadaver tests for practical reasons, while the accelerometers can be fixed in the mouth, it is  
205 possible to apply the *HIC* computation to the head accelerometer data with an approximate 10%  
206 difference (Shang *et al.* 2020b). Evaluation of *UBrIC* (Gabler *et al.* 2018) instead of *BrIC*  
207 (Takhounts *et al.* 2013) would be preferable but was not possible due experimental limitations in the  
208 cadaver tests of (Shang *et al.* 2020b).

## 209 **3. Simulation results**

210 The six staged tests (Shang *et al.* 2020b) were reconstructed and simulated using the MADYMO  
211 platform. Each test was simulated using the three different vehicle contact characteristics (Euro-  
212 NCAP), (Mizuno and Kajzer 2000, Liu *et al.* 2002) and (Martinez *et al.* 2007), see Figure 4.  
213 Pedestrian kinematics and head injury predictions (HIC and BrIC) from vehicle contact and ground  
214 contact were compared between the simulation and the corresponding experiment, see Figure 7 and  
215 Figure 8.

### 216 **3.1. Pedestrian kinematics**

217 The key event timings of the vehicle-pedestrian impact from the staged tests and simulations as well  
218 as the ground contact mechanisms are compared, see Table 3. The ground contact mechanisms are  
219 summarized by assessing the whole-body rotation angles and the posture before landing, with  
220 reference to the definition of (Crocetta *et al.* 2015). Overlaying the video still shots from the  
221 experiments with the simulations was not practical due to camera projection issues. In Test 01 and  
222 Test 02, pedestrian vehicle separation times are generally earlier in the simulations than in the

223 cadaver tests. However, the head ground contacts occurred more than 100ms earlier for the  
 224 simulation in Test 01 but late in Test 02.

225 Table 3-1 Comparison of key events (s) of Test 01

Contact characteristic source	$t_{\text{head-vehicle contact}}$ (s)	$t_{\text{separation}}$ (s)	$t_{\text{head-ground contact}}$ (s)	Ground contact mechanism, from (Crocetta <i>et al.</i> 2015)
Staged test	0.145	0.770	0.995	M1
Mizuno and Liu <sup>1</sup>	0.140	0.595	0.845	M3
Martinez	0.140	0.615	0.875	M3
EU NCAP	0.145	0.610	0.865	M3

226  
227 Table 3-2 Comparison of key events (s) of Test 02

Contact characteristic source	$t_{\text{head-vehicle contact}}$ (s)	$t_{\text{separation}}$ (s)	$t_{\text{head-ground contact}}$ (s)	Ground contact mechanism, from (Crocetta <i>et al.</i> 2015)
Staged test	0.153	0.710	0.986	M3
Mizuno and Liu	0.150	0.625	1.045	M3
Martinez	0.150	0.615	1.020	M3
EU NCAP	0.150	0.655	1.070	M3

228  
229  
230 Table 3-3 Comparison of key events (s) of Test 03

Contact characteristic source	$t_{\text{head-vehicle contact}}$ (s)	$t_{\text{separation}}$ (s)	$t_{\text{head-ground contact}}$ (s)	Ground contact mechanism, from (Crocetta <i>et al.</i> 2015)
Staged test	No show	0.834	1.180	M2
Mizuno and Liu	0.170	0.845	1.1170	M2
Martinez	0.170	0.805	1.1095	M2
EU NCAP	0.160	0.800	1.1130	M2

231  
232 Table 3-4 Comparison of key events (s) of Test 04

Contact characteristic source	$t_{\text{head-vehicle contact}}$ (s)	$t_{\text{separation}}$ (s)	$t_{\text{head-ground contact}}$ (s)	Ground contact mechanism, from (Crocetta <i>et al.</i> 2015)
Staged test	0.169	0.740	0.970	M2
Mizuno and Liu	0.185	0.745	1.030	M2
Martinez	0.185	0.745	1.255	M2
EU NCAP	0.185	0.705	1.190	M2

233  
234 Table 3-5 Comparison of key events (s) of Test 05

Contact characteristic	$t_{\text{head-vehicle contact}}$ (s)	$t_{\text{separation}}$ (s)	$t_{\text{head-ground contact}}$ (s)	Ground contact mechanism, from
------------------------	---------------------------------------	-----------------------------	--------------------------------------	--------------------------------

<sup>1</sup> The contact characteristics used in the simulations are from these authors correspondingly.

source	(Crocetta <i>et al.</i> 2015)			
Staged test	0.098	0.647	0.860	M1
Mizuno and Liu	0.120	0.735	1.790	M1/ M2
Martinez	0.120	0.735	0.990	M1/ M2
EU NCAP	0.115	0.735	1.040	M1/ M2

235

236

Table 3-6 Comparison of key events (s) of Test 06

Contact characteristic source	$t_{\text{head-vehicle contact (s)}}$	$t_{\text{separation (s)}}$	$t_{\text{head-ground contact (s)}}$	Ground contact mechanism, from (Crocetta <i>et al.</i> 2015)
Staged test	0.110	0.727	0.936	M1
Mizuno and Liu	0.135	0.725	0.945	M1/ M2
Martinez	0.135	0.690	0.895	M1/ M2
EU NCAP	0.130	0.680	0.925	M1/ M2

237

238

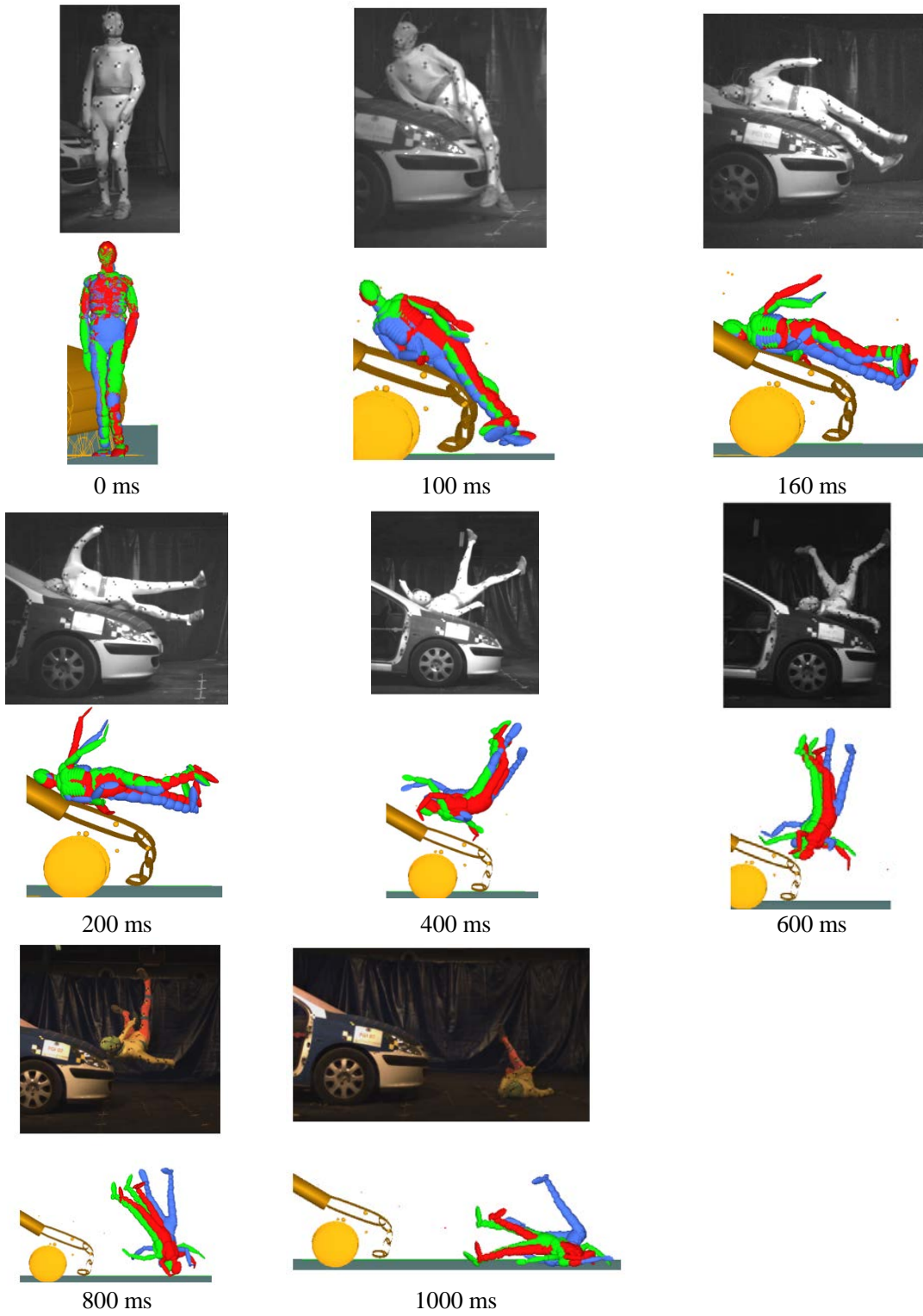


Figure 7-1 Test 01: Sequences of vehicle-pedestrian impact experiment compared with MB simulations. Contact characteristic of vehicle front applied from (Green model: EU NCAP; Blue model: Martinez; Red model: Mizuno)

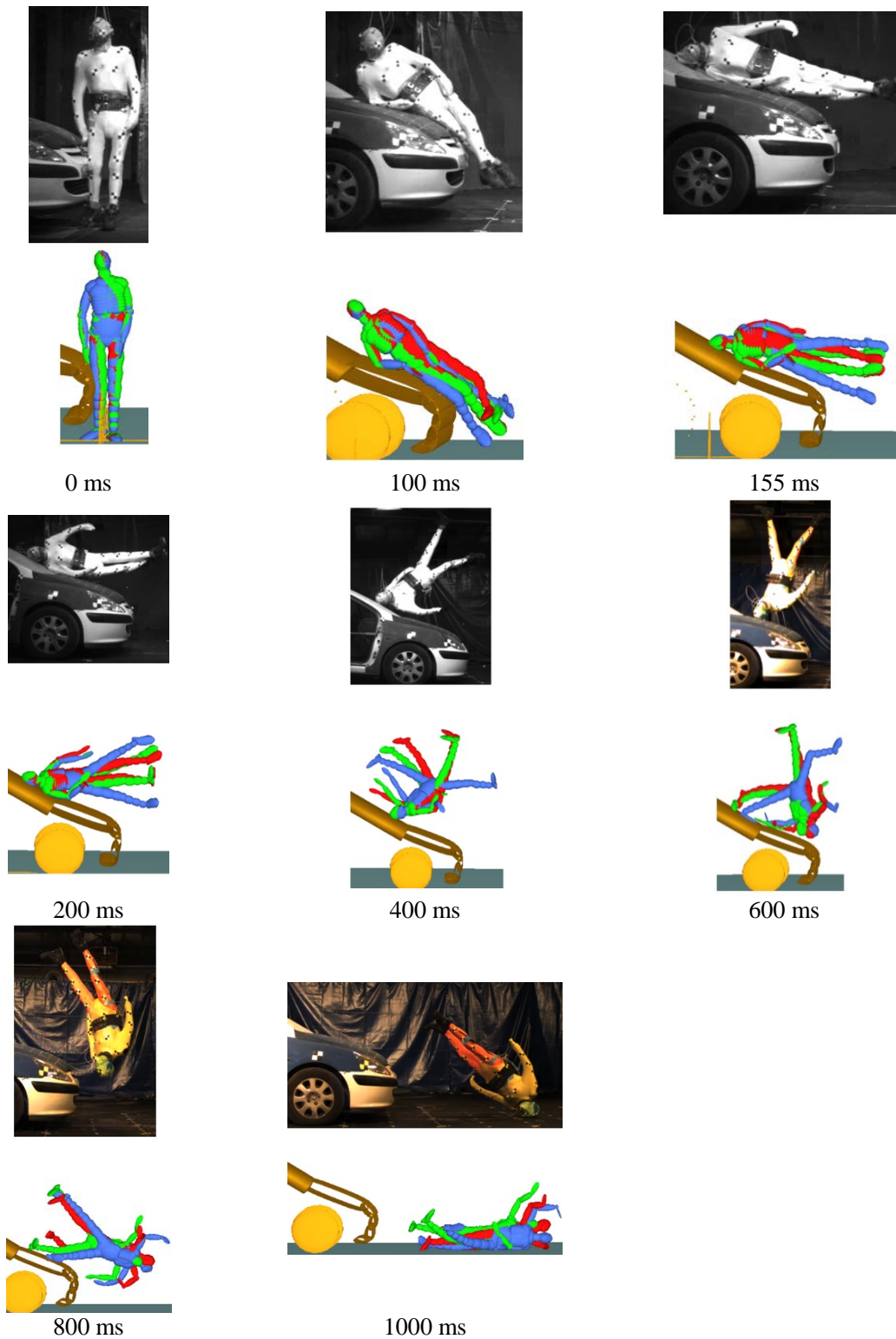


Figure 7-2 Test 02: Sequences of vehicle-pedestrian impact experiment compared with MB simulations. Contact characteristic of vehicle front applied from (Green model: EU NCAP; Blue model: Martinez; Red model: Mizuno)

242  
243



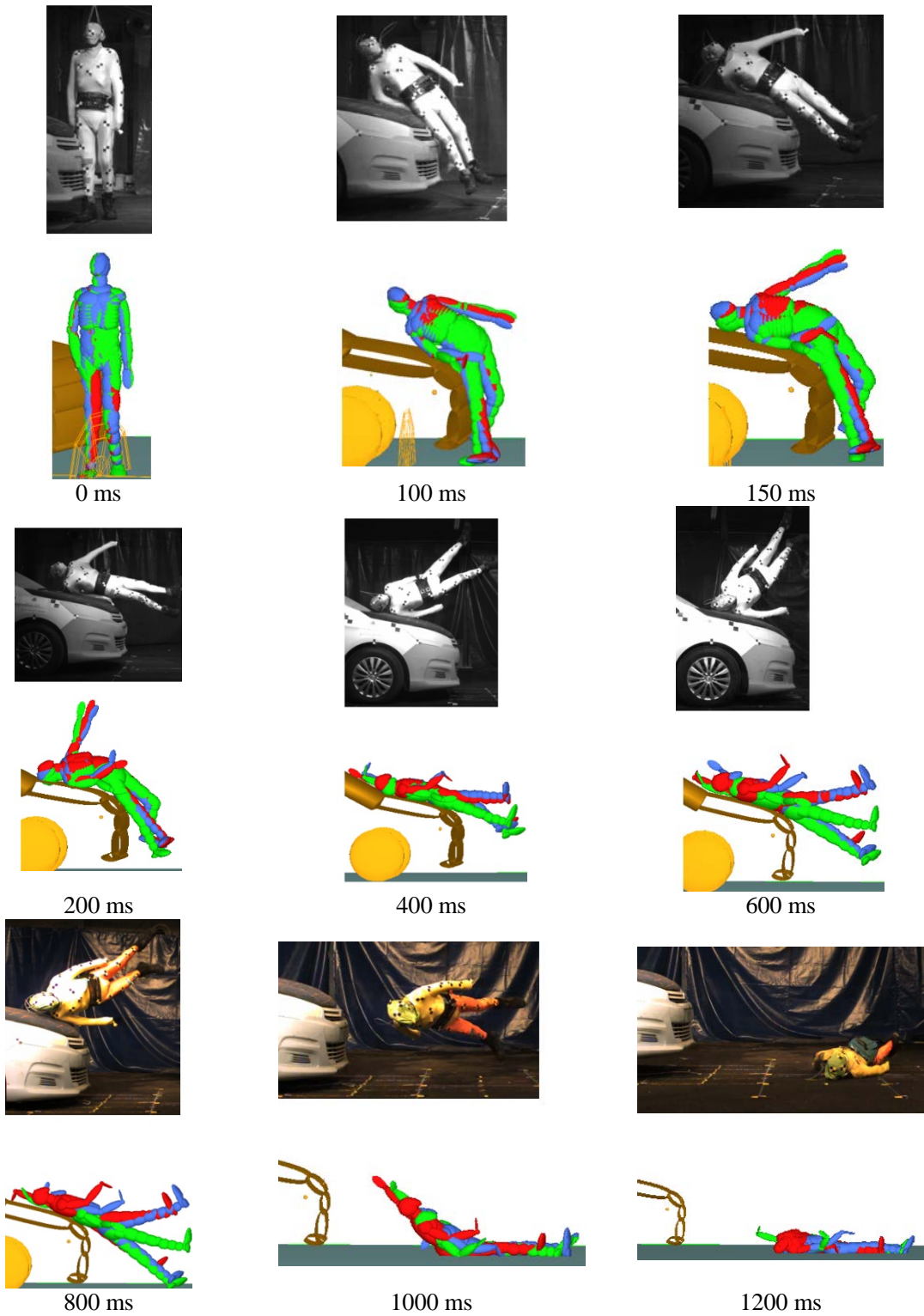


Figure 7-3 Test 03: Sequences of vehicle-pedestrian impact experiment compared with MB simulations. Contact characteristic of vehicle front applied from (Green model: EU NCAP; Blue model: Martinez; Red model: Mizuno)

244  
245  
246

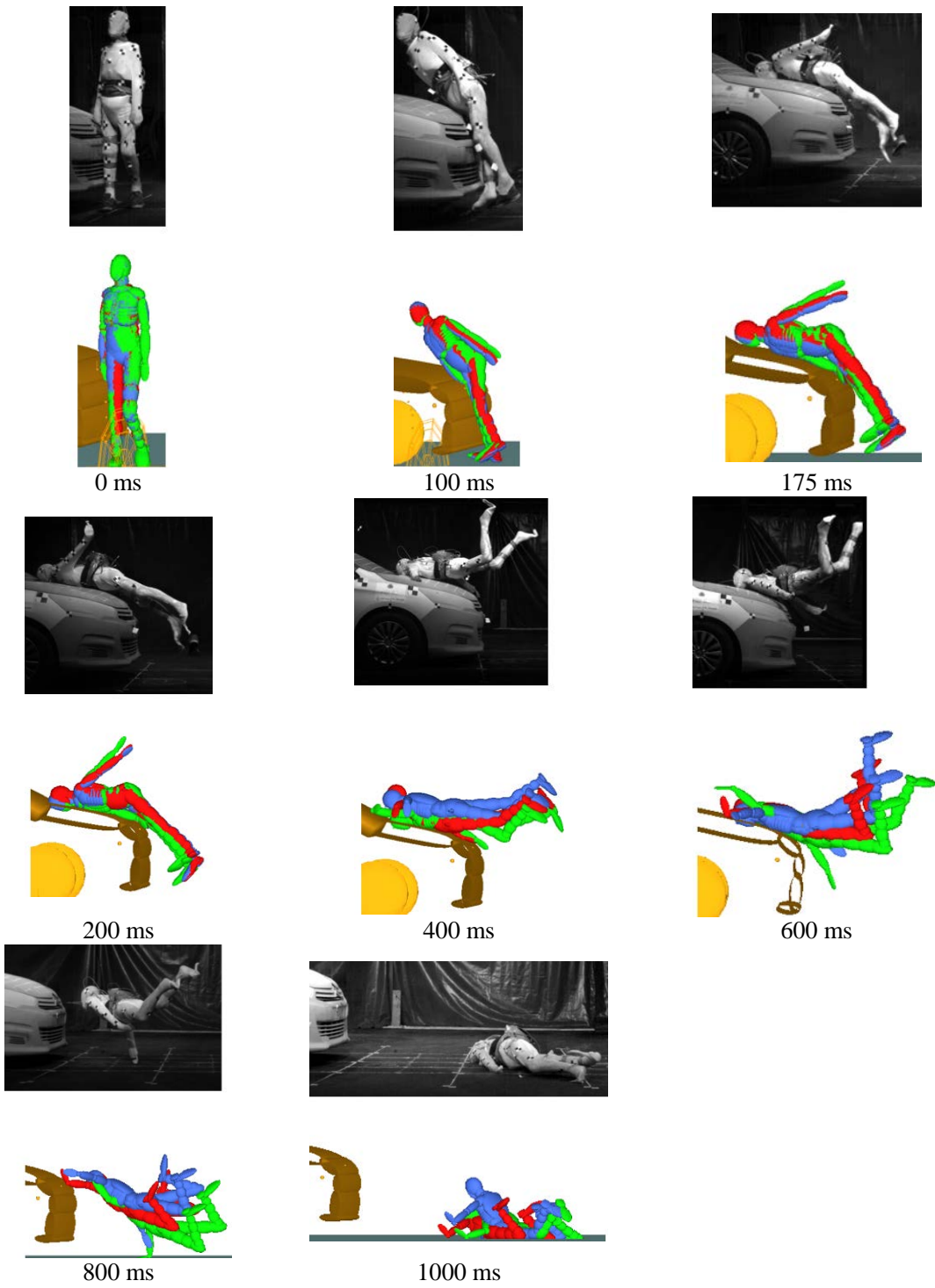


Figure 7-4 Test 04: Sequences of vehicle-pedestrian impact experiment compared with MB simulations. Contact characteristic of vehicle front applied from (Green model: EU NCAP; Blue model: Martinez; Red model: Mizuno)

247  
248

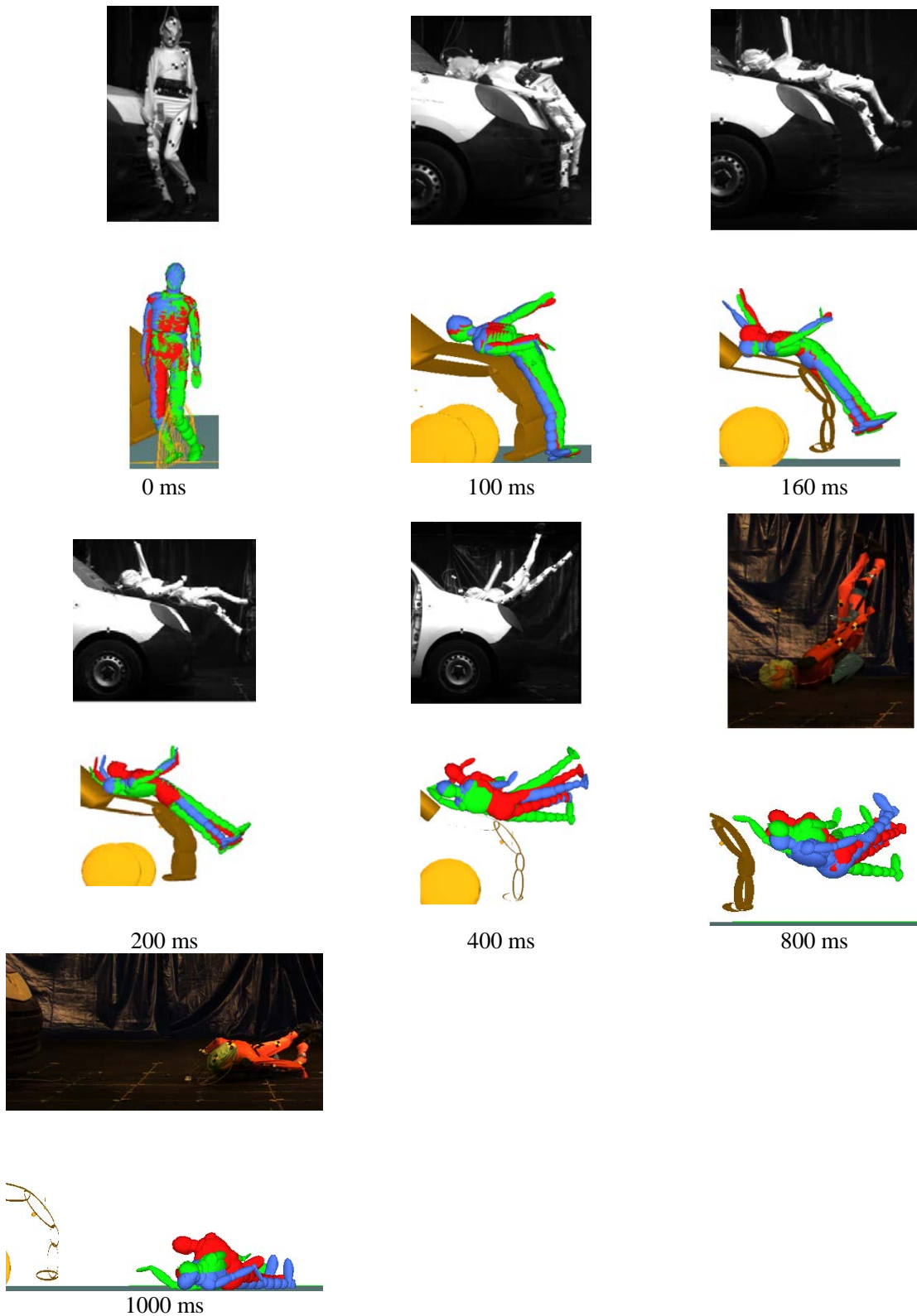


Figure 7-5 Test 05: Sequences of vehicle-pedestrian impact experiment compared with MB simulations. Contact characteristic of vehicle front applied from (Green model: EU NCAP; Blue model: Martinez; Red model: Mizuno)

249  
250

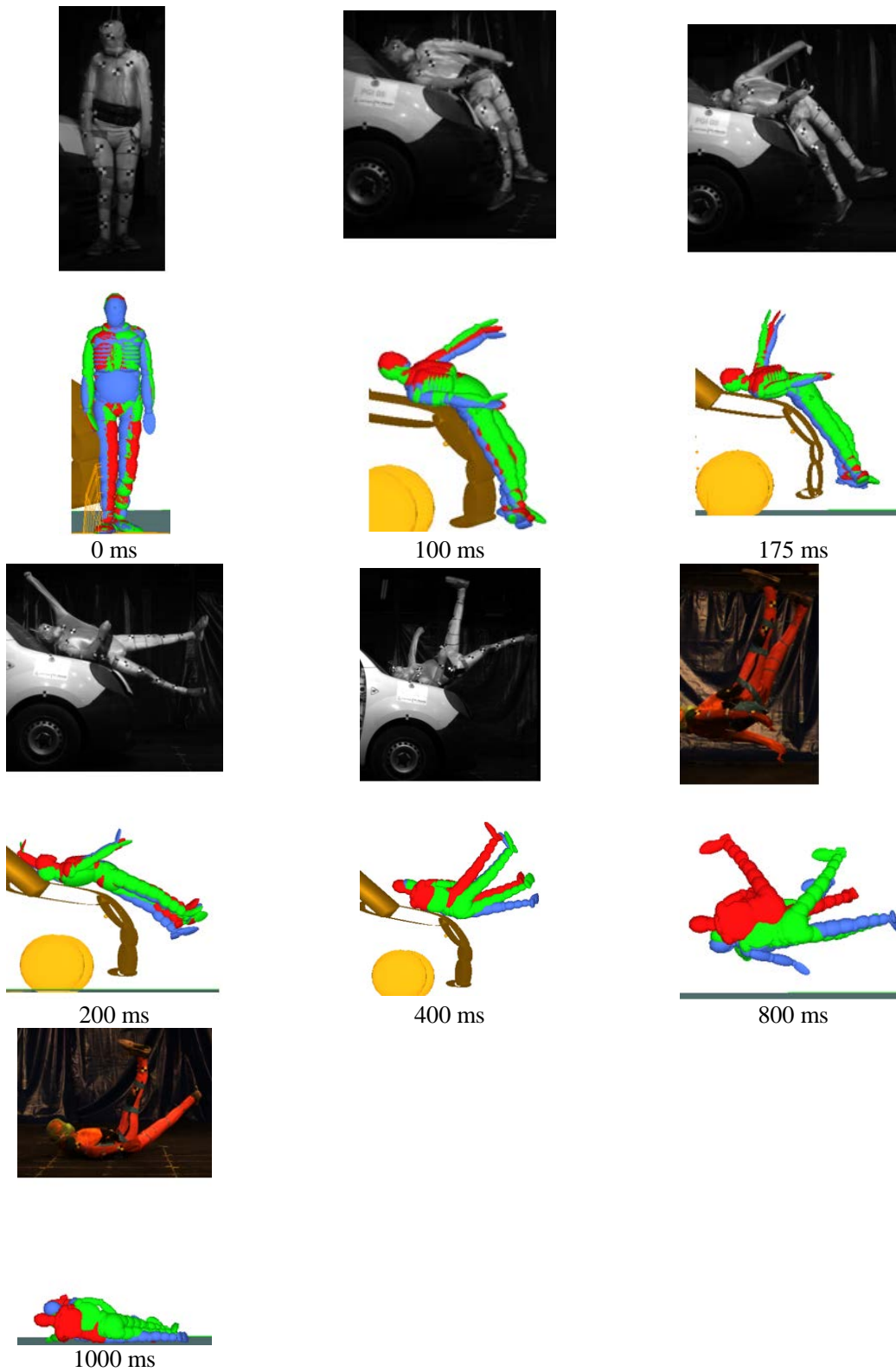


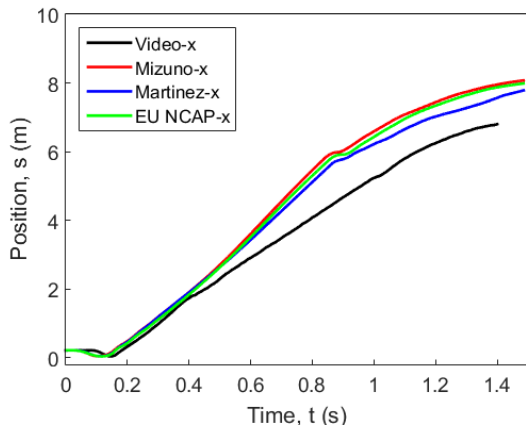
Figure 7-6 Test 06: Sequences of vehicle-pedestrian impact experiment compared with simulations. Contact characteristic of vehicle front applied from (Green model: EU NCAP; Blue model: Martinez; Red model: Mizuno)

251  
252

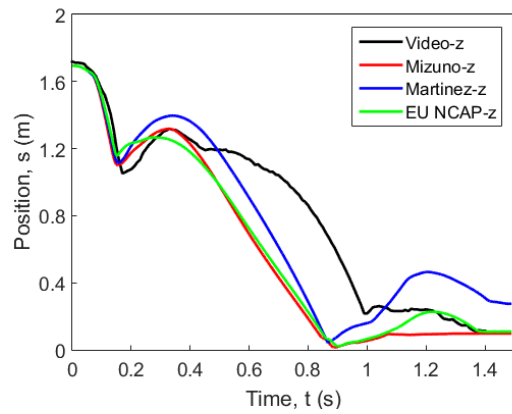
253 **3.2. Pedestrian planar head trajectories**

254 Pedestrian planar head trajectories (tracked based on the marker on pedestrian forehead) in both the  
 255 X (horizontal, positive direction of vehicle travel) and Z (vertically upwards) directions from staged  
 256 tests and the simulations are compared, see Figure 8. Appendix Figure B1 shows the definition of the  
 257 coordinate system after (Shang *et al.* 2020b). For Test 01 and Test 02, the horizontal head motion in  
 258 the simulations is greater than was observed in the experiments.

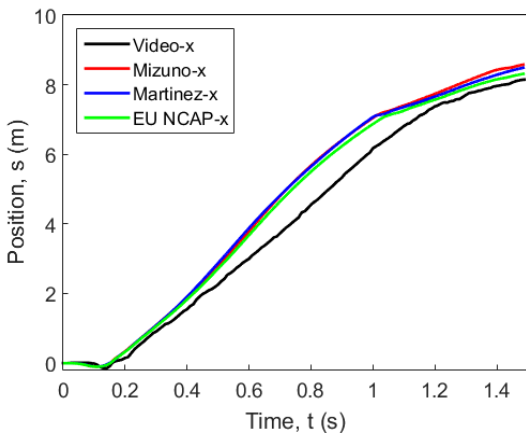
259



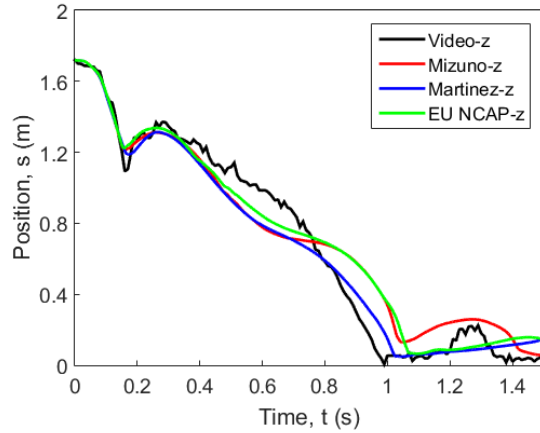
(a) Head marker-x T1



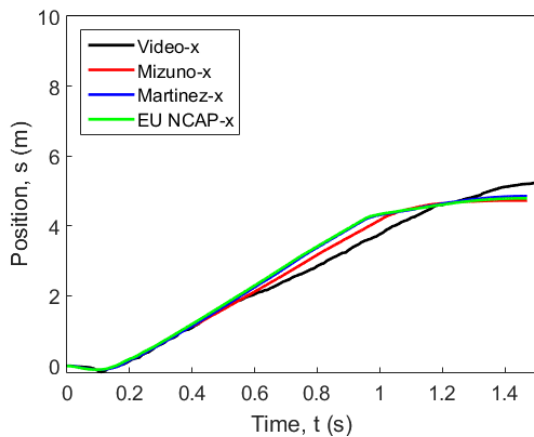
(b) Head marker -z T1



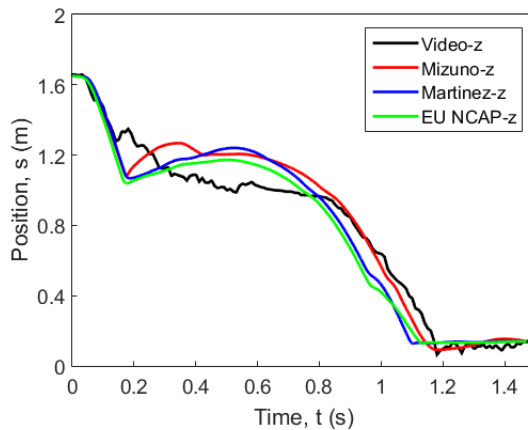
(c) Head marker-x T2



(d) Head marker -z T2



(e) Head marker-x T3



(f) Head marker -z T3

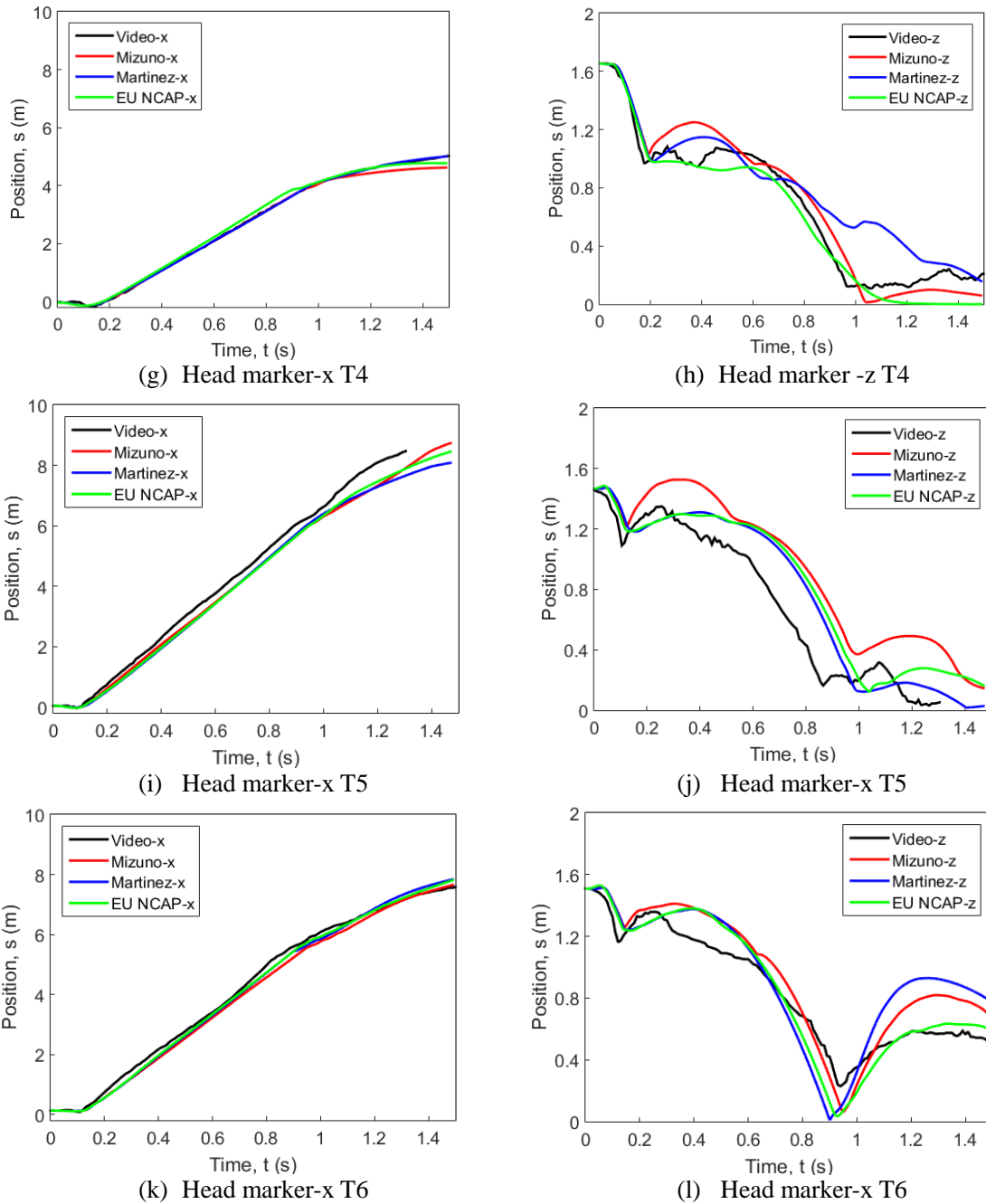
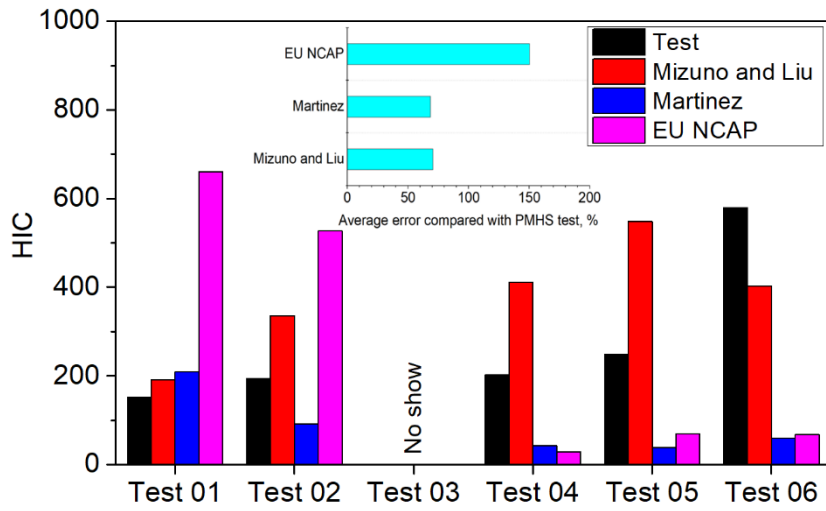


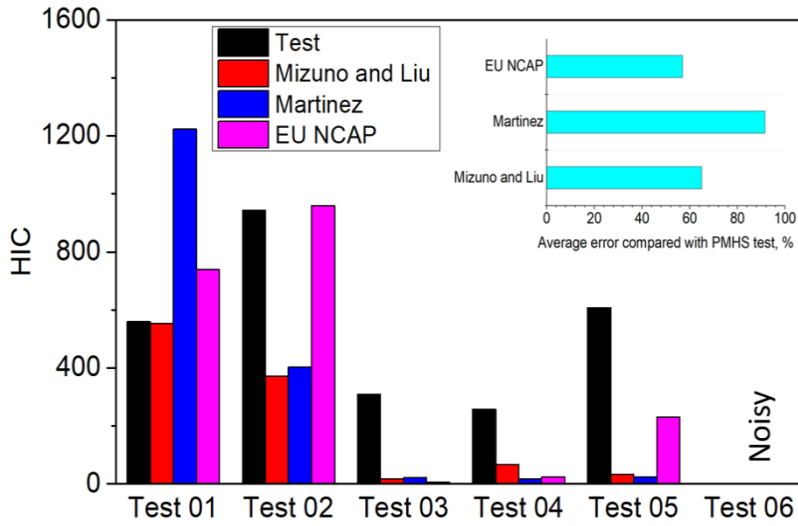
Figure 8 Comparison of pedestrian forehead trajectories between cadaver experiments and simulations

260 **3.3. Pedestrian head injury criteria assessments**

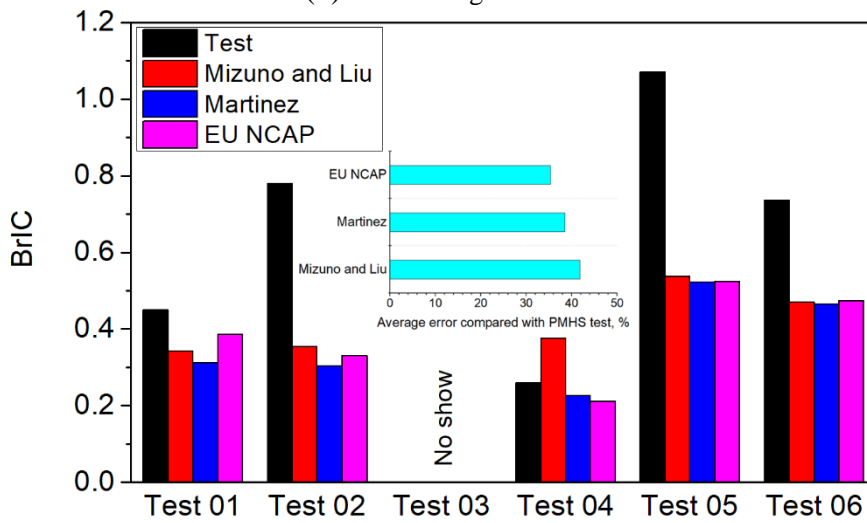
261 The *HIC* and *BrIC* scores were calculated for both vehicle and ground contact for all six cases and  
 262 compared with the staged PMHS test results, as shown in Figure 9. The average errors for the injury  
 263 indices for both vehicle and ground contact over all six tests obtained from simulations using vehicle  
 264 contact characteristics from Mizuno and Liu, Martinez and EU NCAP compared with the cadaver  
 265 tests are 51.3%, 62.0%, 73.3%, respectively.



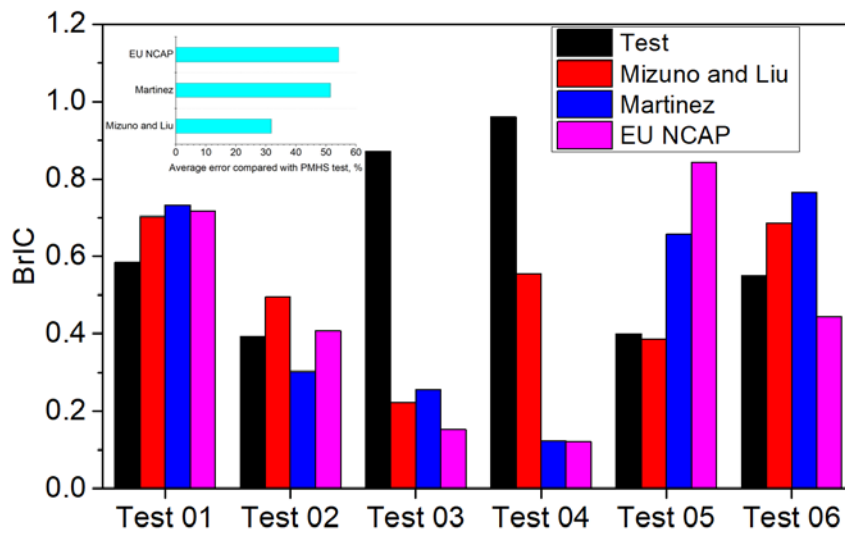
(a) *HIC* from vehicle contact



(b) *HIC* from ground contact



(c) *BrIC* from vehicle contact



(d) *BrIC* from ground contact

Figure 9 Comparison of head injury indices from vehicle and ground contact

267 **4. Sensitivity study**

268 The vehicle contact characteristics do not obviously affect the kinematics during the vehicle contact.  
 269 However, Section 3.3 shows they do have a large influence on the secondary ground contact and the  
 270 resulting injury predictions. The influence of the pedestrian initial joint angles and internal damping  
 271 of the MADYMO pedestrian model are also of interest. In these sensitivity studies, the Mizuno and  
 272 Liu's stiffness was used as the baseline for comparisons as this stiffness gave the smallest overall  
 273 error, see Figure 9.

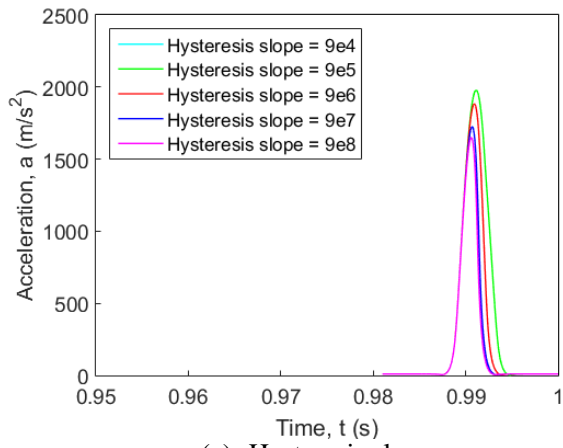
274

275 **4.1. Sensitivity study of hysteresis and unloading curve**

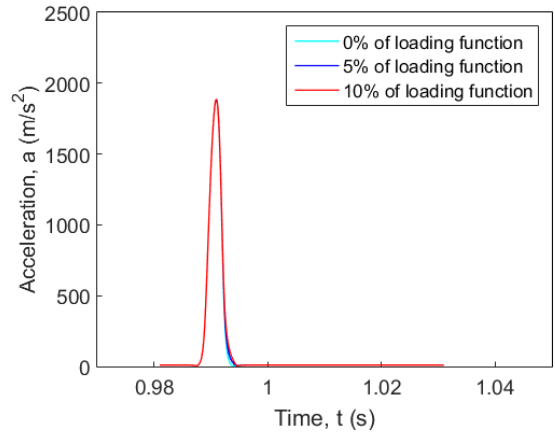
276 Apart from the loading function, the hysteresis slope and unloading curve definitions in MADYMO  
 277 further influence the contact modelling. The effects were tested based on the simplified head model  
 278 impact simulations. The hysteresis slope over 5 magnitudes (9e4, 9e5, 9e6, 9e7 and 9e8) and the  
 279 unloading curves in 3 different ratios (0%, 5% and 10%) of loading curve were tested, see Figure 10.  
 280 Results showed that lower hysteresis slopes produced relatively higher acceleration peaks and wider  
 281 waves which can greatly impact *HIC* scores. Altering the unloading curve showed a negligible effect  
 282 on the peak and impact time duration.

283





(a) Hysteresis slope



(b) Unloading curve (hysteresis slope =  $9e6$ )

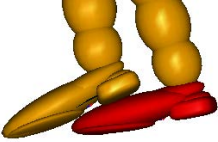
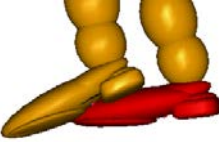
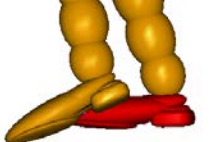
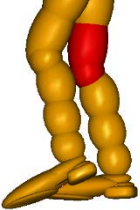
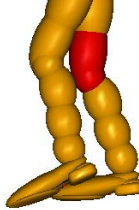
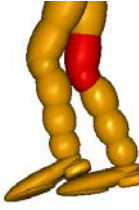



Figure 10 Testing of hysteresis slope and unloading curve effect on the contact using a simplified sphere model

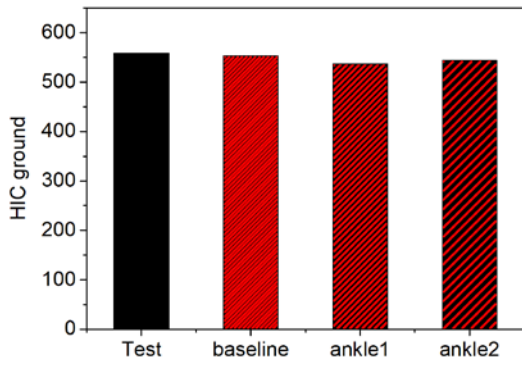
285

286 **4.2. Sensitivity study of pedestrian initial joint angle**

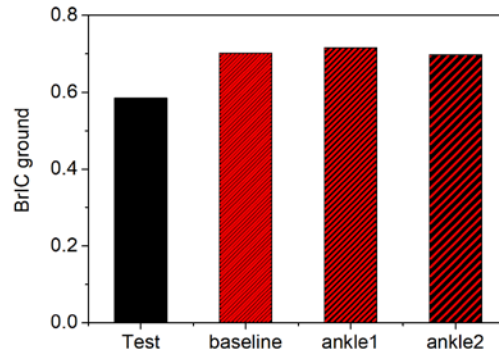
287 The initial joint postures of the MADYMO pedestrian model were set based on the measurement of  
288 the joint angles of captured images in different views of the cadavers just before testing (Shang *et al.*  
289 2020b). The effect of the joint angles was studied to assess the influence of joint angle on the  
290 resulting kinematics. Considering Test 01, the initial hip angle, knee angle and ankle angle of the  
291 struck leg were changed  $\pm 5$  degrees in YZ plane (see Table 4) to check the influence on the ground  
292 related head injury indices. Only one parameter was changed each time and the other two were kept  
293 constant (baseline) for this sensitivity study. The results are shown in Figure 11. The injury indices  
294 obtained from the baseline model and the pedestrian with initial joint angle 2 (as illustrated in Table  
295 4) are close while for the pedestrian with initial hip joint angle 2 and knee joint angle 2, the injuries  
296 showed noticeable differences when compared with the baseline results, as did the ground contact  
297 mechanisms, see Figure 12.

Table 4 Initial angles of joint sensitivity study

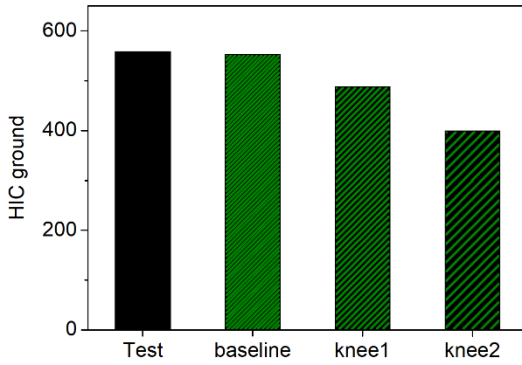
Joint	Angle 1 (-5°)	Baseline angle (°)	Angle 2 (+5°)
	2	7	12
Ankle			
	21	26	31
Knee			
	-5	0	5
Hip			



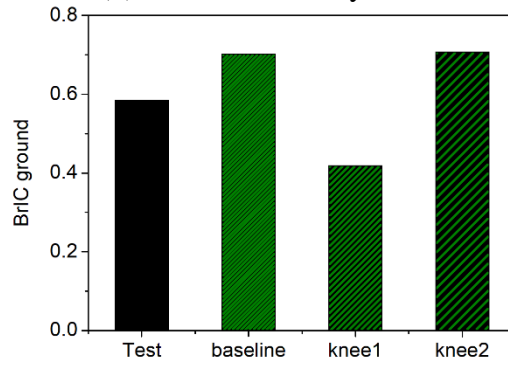
(a) Ankle sensitivity for *HIC*



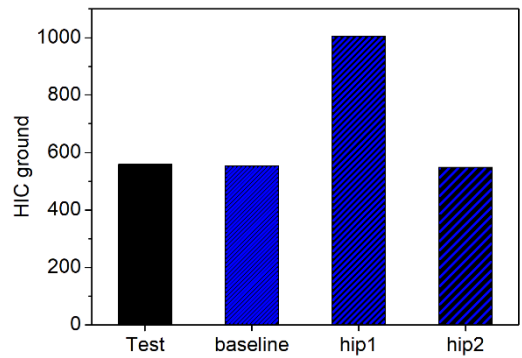
(b) Ankle sensitivity for *BrIC*



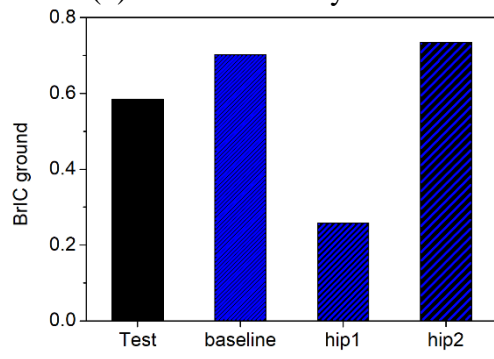
(c) Knee sensitivity for *HIC*



(d) Knee sensitivity for *BrIC*



(e) Hip sensitivity for *HIC*



(f) Hip sensitivity for *BrIC*

Figure 11 Initial joint angle effect on *HIC* and *BrIC* from ground contact for Test 01

298

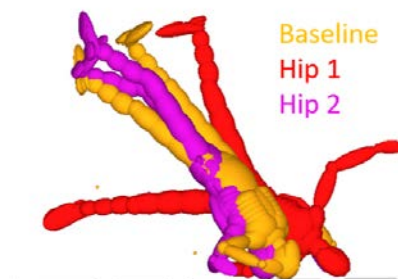


Figure 12 Pedestrian ground contact mechanisms in Test 01 from different initial hip angle from Table

299 **4.3. Sensitivity study of bending of pedestrian model**

300 As seen in Test 01 and Test 02 shown in Figure 7, the pedestrian model bounced off the vehicle after  
301 the head windscreen impact, but this did not occur in the cadaver tests. A potential reason for the  
302 excessive bouncing could be insufficient internal damping in the pedestrian models. A sensitivity  
303 study of human model bending was therefore performed, with a modified a damping coefficient of  
304 100 N·s/m used to reconstruct Test 01 and compared with the baseline simulation (almost no  
305 damping), see Figure 13. The damping added to the model did not significantly reduce the rebound  
306 but did significantly change the post-impact kinematics and the mechanism of ground contact.  
307

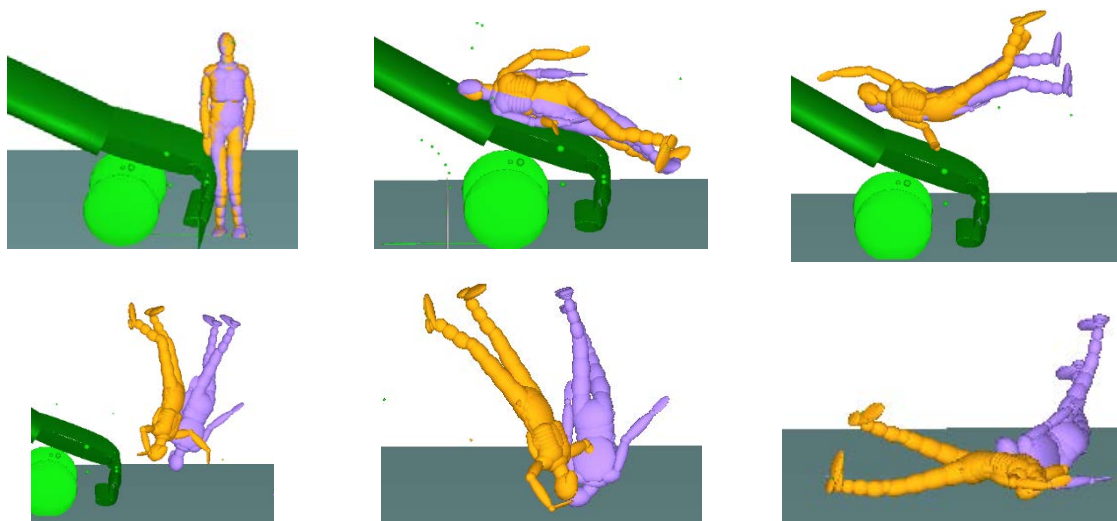


Figure 13 Sequence of baseline pedestrian model (orange) and the model with added damping kinematics (purple) in vehicle crash for Test 01

308

309 **5. Discussion**

310 This paper presents the first kinematics assessment of a multibody pedestrian impact model for the  
311 phases following vehicle impact up to and including the ground contact, using cadaver test data for  
312 comparison.

313

314 A computational model for assessing pedestrian ground contact injuries, and for possible use in the  
315 development of ground contact injury prevention countermeasures, has a number of hierarchical  
316 requirements. In terms of whole-body kinematics, there is the need for replicating the main body  
317 segment trajectories following the initial vehicle contact, followed by the pre-impact pose and

318 velocity for the ground contact, especially the head. Subsequently, replicating the 6 DOF motion of  
319 the head and other body segments during ground contact is needed for injury criteria evaluation. For  
320 finite element models, tissue level stress/strain responses can be assessed, but this is beyond the  
321 scope of the current paper which focuses on the evaluation of the multibody MADYMO ellipsoid  
322 pedestrian model.

323

324 Table 3 shows that the timings of the head to vehicle contact are well reproduced for Test 01 and Test  
325 02 of Shang et al 2020, where the collision speed is 30 kph and the normalized bonnet leading-edge  
326 height is 0.7. However, for the 20kph cases (Tests 03 and 04) and the two high bonnet cases at 30  
327 kph (Tests 05 and 06), there are substantial differences (of the order of 20 ms) in the head to vehicle  
328 contact times. For Tests 01 and 02 the models separate from the vehicle too early, showing evidence  
329 of insufficient energy absorption. However neither varying the contact characteristics nor introducing  
330 additional damping was successful in addressing this. The timing of the subsequent ground contact is  
331 poor in some cases (maximum error is 0.9s in Test 05, see Table 3-5, the arm of the pedestrian model  
332 prevented the head impacting the ground) but the correspondence to the pedestrian ground contact  
333 mechanisms identified by (Crocetta *et al.* 2015) is reasonable (correct mechanism identified in three  
334 cases, incorrect in one case, and partially correct in two cases. However, Figure 7 shows some  
335 substantial differences in the flight trajectory and ground contact sequences. In consequence it is not  
336 surprising that the resulting injury criteria assessments in Figure 9 show cases where very substantial  
337 differences between the model and the corresponding experiment are evident. Thus the current  
338 MADYMO pedestrian models cannot reliably distinguish the influence of the various factors varying  
339 between the different tests (vehicle shape and speed, body size and pose, vehicle contact  
340 characteristic).

341

342 The sensitivity studies show that the choice of vehicle contact characteristic makes a significant  
343 difference to pedestrian ground contact kinematics and injury evaluations, as do the hysteresis slope  
344 and the initial knee and hip angles. Somewhat surprisingly, the contact characteristic using the older  
345 data from impactor tests by Mizuno and Liu generally yielded the lowest errors for *HIC* in the  
346 vehicle contact (Figure 9a), but the reliability of the resulting ground contact *HIC* is poor (Figure

347 9b). Similarly, the predictions of the *BrIC* in both the vehicle and ground contacts are a poor match  
348 to the experimental data.

349  
350 Increasing the internal damping in the pedestrian model does affect the kinematics but did not  
351 improve the comparison with the experimental data. A further round of simulations was conducted  
352 with the goal of improving the match between the predicted and test ground impact mechanisms by  
353 changing the vehicle contact stiffness. The results are not presented here, but the outcome was that  
354 while this approach was successful in improving the ground contact kinematics, the resulting vehicle  
355 contact injury predictions were very different to the experiments.

356  
357 Accordingly, future work must focus on amendments to the MADYMO pedestrian model to improve  
358 its predictive capacity and ground contact, and on assessing the predictive capacity of other  
359 multibody and finite element model formulations (Maeno and Hasegawa 2001, Iwamoto *et al.* 2003,  
360 Untaroiu *et al.* 2016). This is needed before the model can be confidently applied to assess ground  
361 contact injury countermeasures (for example about technology or vehicle front shape changes).  
362 Similarly, it is clear that the MADYMO pedestrian model currently has limited potential for  
363 application to individual collision reconstruction purposes, though there have been substantial  
364 applications of this in the literature (Shen and Jin 2008).

## 365 366 **6. Limitations**

367 There are several limitations to this study. Firstly, the experimental data is based on cadaver testing  
368 and it is understood that a living human response would be different, especially for the two 20kph  
369 tests where voluntary motion is likely to play a significant role. Only one pedestrian model  
370 formulation was assessed, and it is possible that a different multibody or a finite element model  
371 would perform better. The models were globally scaled based on height and mass, not as an  
372 individual body segment level. The experimental measurements of the pre-impact joint angles of the  
373 cadavers were not precisely known.

## 374 375 **7. Conclusions**

376 We have presented the first assessment of a computational model (here the MADYMO ellipsoid

377 multibody pedestrian model) for predicting pedestrian flight and ground contact following a vehicle  
378 collision. A comparison with six cadaver tests performed over the speed range 20-30kph and with  
379 three different vehicle types and pedestrian sizes showed good capacity to predict vehicle contact  
380 times, but differences between the models and experiments manifested prior to vehicle pedestrian  
381 separation, and resulted in considerable differences in the ground contact kinematics. The resulting  
382 head injury predictions based on the ground contact *HIC* and *BrIC* scores showed limited capacity of  
383 the model to replicate individual experiments. Sensitivity studies showed substantial influences of  
384 the vehicle- pedestrian contact characteristic and some of the initial pedestrian joint angles on the  
385 subsequent ground contact injury predictions. Further work is needed to improve the predictive  
386 capacity of the MADYMO pedestrian model for ground contact injury predictions.

387

### 388 ***Acknowledgement***

389 The authors would like to thank EURONCAP for generous provision of the impactor data. The  
390 support of the China Scholarship Council (CSC) is highly appreciated.

391

392

### 393 ***References***

394

395 Barry, F., Simms, C., 2016. Assessment of head - ground impact patterns in real world pedestrian - vehicle  
396 collisions. In: Proceedings of the IRCOBI Conference Proceedings.

397 Crocetta, G., Piantini, S., Pierini, M., Simms, C., 2015. The influence of vehicle front-end design on pedestrian  
398 ground impact. *Accident Analysis and Prevention* 79, 56-69.

399 Delange, R., Vanrooij, L., Happee, R., Liu, X., 2006. Validation of human pedestrian models using laboratory  
400 data as well as accident reconstruction.

401 Elliott, J., Simms, C., Wood, D., 2012. Pedestrian head translation, rotation and impact velocity: The influence  
402 of vehicle speed, pedestrian speed and pedestrian gait. *Accident Analysis Prevention* 45, 342-353.

403 Euro-Ncap, <https://www.euroncap.com>.

404 Euro-Ncap, 2010. Pedestrian testing protocol.

405 Gabler, L.F., Crandall, J.R., Panzer, M.B., 2018. Development of a metric for predicting brain strain responses  
406 using head kinematics. *Annals of biomedical engineering* 46 (7), 972-985.

407 Han, Y., Li, Q., Wang, F., Wang, B., Mizuno, K., Zhou, Q., 2018. Analysis of pedestrian kinematics and ground  
408 impact in traffic accidents using video records. *International Journal of Crashworthiness*, 1-10.

409 Hobbs, C.A., Mcdonough, P.J., 1998. Development of the european new car assessment programme (euro  
410 ncap). *Regulation* 44, 3.

411 Ishikawa, H., Kajzer, J., Schroeder, G., 1993. Computer simulation of impact response of the human body in

412 car-pedestrian accidents. SAE Technical Paper.

413 Iwamoto, M., Omori, K., Kimpara, H., Nakahira, Y., Tamura, A., Watanabe, I., Miki, K., Hasegawa, J., Oshita,  
414 F., Nagakute, A., 2003. Recent advances in thums: Development of individual internal organs, brain,  
415 small female and pedestrian model. In: Proceedings of the Proceedings of 4th European LS Dyna  
416 Users conference, pp. 1-10.

417 Kajzer, J., Cavallero, C., Bonnoit, J., Morjane, A., Ghanouchi, S., 1993. Response of the knee joint in lateral  
418 impact: Effect of bending moment. In: Proceedings of the Proceedings of the IRCOBI Conference, pp.  
419 105-116.

420 Kerrigan, J.R., Crandall, J.R., Deng, B., 2007. Pedestrian kinematic response to mid-sized vehicle impact.  
421 International journal of vehicle safety 2 (3), 221-240.

422 Khaykin, A., Lerner, D.L., 2016. Adhesive vehicle front end for mitigation of secondary pedestrian impact.  
423 Google Patents.

424 Li, G., Wang, F., Otte, D., Cai, Z., Simms, C., 2018. Have pedestrian subsystem tests improved passenger car  
425 front shape? Accident Analysis Prevention 115, 143-150.

426 Li, G., Yang, J., Simms, C., 2016. A virtual test system representing the distribution of pedestrian impact  
427 configurations for future vehicle front-end optimization. Traffic Injury Prevention 17 (5), 515-523.

428 Liu, X.J., Yang, J.K., Lövsund, P., 2002. A study of influences of vehicle speed and front structure on  
429 pedestrian impact responses using mathematical models. Traffic Injury Prevention 3 (1), 31-42.

430 Maeno, T., Hasegawa, J., 2001. Development of a finite element model of the total human model for safety  
431 (thums) and application to car-pedestrian impacts. SAE Technical Paper.

432 Martinez, L., Guerra, L.J., Ferichola, G., Garcia, A., Yang, J., 2007. Stiffness corridors of the european fleet for  
433 pedestrian simulations. In: Proceedings of the 20th International Technical Conference on the  
434 Enhanced Safety of Vehicles (ESV) National Highway Traffic Safety Administration.

435 Mizuno, K., Kajzer, J., 2000. Head injuries in vehicle-pedestrian impact. SAE Technical paper.

436 Shang, S., 2020. Pedestrian whole body ground contact mechanisms and head injury assessment following  
437 vehicle impact. Trinity College Dublin.

438 Shang, S., Masson, C., Teeling, D., Py, M., Ferrand, Q., Arnoux, P.-J., Simms, C., 2020a. Kinematics and  
439 dynamics of pedestrian head ground contact: A cadaver study. Safety Science 127, 104684.

440 Shang, S., Masson, C., Teeling, D., Py, M., Ferrand, Q., Arnoux, P.-J., Simms, C.J.S.S., 2020b. Kinematics  
441 and dynamics of pedestrian head ground contact: A cadaver study. 127, 104684.

442 Shang, S., Otte, D., Li, G., Simms, C., 2018. Detailed assessment of pedestrian ground contact injuries  
443 observed from in-depth accident data. Accident Analysis & Prevention 110, 9-17.

444 Shen, J., Jin, X., 2008. Improvement in numerical reconstruction for vehicle—pedestrian accidents. In:  
445 Proceedings of the Proceedings of the Institution of Mechanical Engineers, Part D: Journal of  
446 Automobile Engineering, pp. 25-39.

447 Shi, L., Han, Y., Huang, H., He, W., Wang, F., Wang, B., 2019. Effects of vehicle front-end safety  
448 countermeasures on pedestrian head injury risk during ground impact. Proceedings of the Institution  
449 of Mechanical Engineers, Part D: Journal of Automobile Engineering, 0954407019828845.

450 Simms, C.K., Wood, D.P., 2006. Effects of pre-impact pedestrian position and motion on kinematics and  
451 injuries from vehicle and ground contact. International Journal of Crashworthiness 11 (4), 345-355.

452 Takhounts, E.G., Craig, M.J., Moorhouse, K., Mcfadden, J., Hasija, V., 2013. Development of brain injury  
453 criteria (bric). SAE Technical Paper.

454 The-Blueprints, <http://www.the-blueprints.com/>.

455 Triana, C., Fajardo, F., 2013. Experimental study of simple harmonic motion of a spring-mass system as a



456 function of spring diameter. *Revista Brasileira de Ensino de Física* 35 (4), 1-8.

457 Untaroiu, C.D., Meissner, M.U., Crandall, J.R., Takahashi, Y., Okamoto, M., Ito, O., 2009. Crash reconstruction  
458 of pedestrian accidents using optimization techniques. *International Journal of Impact Engineering* 36  
459 (2), 210-219.

460 Untaroiu, C.D., Putnam, J.B., Schap, J., Davis, M.L., Gayzik, F.S., 2016. Development and preliminary  
461 validation of a 50th percentile pedestrian finite element model. In: *Proceedings of the ASME 2015*  
462 *International Design Engineering Technical Conferences and Computers and Information in*  
463 *Engineering Conference*.

464 Van Hoof, J., De Lange, R., Wismans, J.S., 2003. Improving pedestrian safety using numerical human  
465 models. *SAE Technical Paper*.

466 Van Rooij, L., Bhalla, K., Meissner, M., Ivarsson, J., Crandall, J., Longhitano, D., Takahashi, Y., Dokko, Y.,  
467 Kikuchi, Y., 2003. Pedestrian crash reconstruction using multi-body modeling with geometrically  
468 detailed, validated vehicle models and advanced pedestrian injury criteria. In: *Proceedings of the 18th*  
469 *ESV Conference*.

470 Who, 2018. *Global status report on road safety 2018* World Health Organization.

471 Who, <https://extranet.who.int/roadsafety/death-on-the-roads/#ticker>.

472 Xu, J., Shang, S., Yu, G., Qi, H., Wang, Y., Xu, S., 2016. Are electric self-balancing scooters safe in vehicle  
473 crash accidents? *Accident Analysis & Prevention* 87, 102-116.

474 Yang, J., Kajzer, J., Cavallero, C., Bonnoit, J., 1995. Computer simulation of shearing and bending response  
475 of the knee joint to a lateral impact. *SAE Technical Paper*.

476 Yang, J., Lovsund, P., 1997. Development and validation of a human-body mathematical model for simulation  
477 of car-pedestrian collisions. In: *Proceedings of the Proc. of the Int. IRCOBI Conf., Hanover*  
478 *(Germany)*, pp. 133-49.

479 Yang, J., Rzymkowski, C., Kajzer, J., 1993. Development and validation of a mathematical breakable leg  
480 model. In: *Proceedings of the Proceedings of the International Research Council on the*  
481 *Biomechanics of Injury conference*, pp. 175-186.

482 Yao, J., Yang, J., Otte, D., 2008. Investigation of head injuries by reconstructions of real-world vehicle-versus-  
483 adult-pedestrian accidents. *Safety science* 46 (7), 1103-1114.

484 Zou, T., Shang, S., Simms, C., 2019. Potential benefits of controlled vehicle braking to reduce pedestrian  
485 ground contact injuries. *Accident Analysis & Prevention* 129, 94-107.

486

Table A1 Summary of tests performed in (Shang et al. 2020a)

Test number	Vehicle model	Vehicle speed (km/h)	Pedestrian age (y/o)	Pedestrian sex	Pedestrian height (m)	Pedestrian mass (kg)	NBLEH
Test 01	Peugeot 307	30.5	88	Male	1.74	66	0.7
Test 02	Peugeot 307	30.4	83	Male	1.72	69	0.7
Test 03	Citroen C4	20.4	94	Male	1.67	64	0.9
Test 04	Citroen C4	21.0	83	Male	1.67	55	0.9
Test 05	Renault Kangoo II	30.1	94	Female	1.58	38	1.2
Test 06	Renault Kangoo II	30.4	86	Male	1.62	69	1.1

490

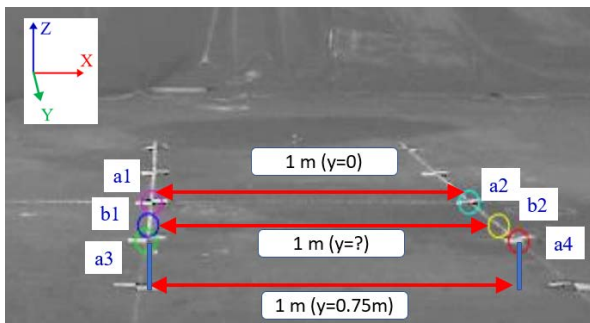
491 **Appendix B: Steps of defining and validating the movement input of the MB vehicle models**

492

493 (1) According to the width of the vehicle and the markers on the lab ground, using ginput  
494 function in Matlab to pick 2 pairs of points (a1 and a2, a3 and a4) which define 1 m in  $y=0$   
495 and  $y=0.75$ , then the scale (the length of b1b2, the coordinates of b1 and b2 are in line with  
496 the coordinates of the reference points picked from the side of the vehicle) can be calculated  
497 based on the mathematical relation, see Figure B1 (a). The scale in Y direction depends on  
498 the coordinates of the points P1 and P2 in Figure B1 (b).

499 (2) P1 is a reference point which can be used to find the tracking point P0 based on their relative  
500 positional relationship. Pick two points P1 and P2 in a line on the side of the vehicle, then the  
501 angular change of the vehicle can be calculated.

502



(a) Demonstration of choosing the scale



(b) Demonstration of choosing the tracking point P0

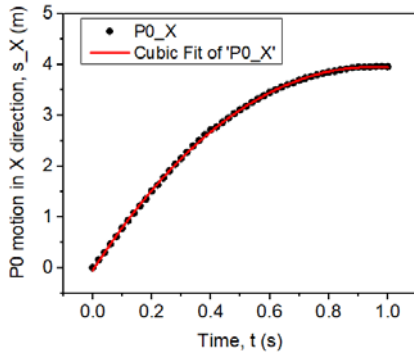
Figure B1: The steps of choosing the tracking point

503

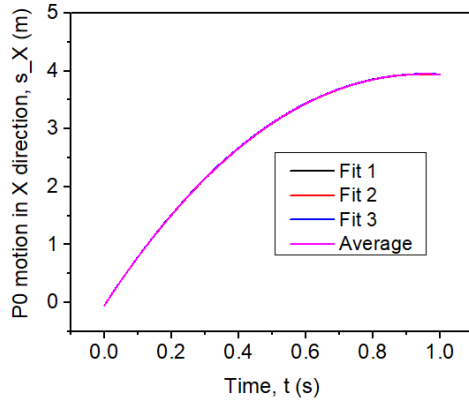
504 After the X and Z motion of the tracking point and the angle of the vehicle were calculated, the  
505 polynomial fittings (third-degree polynomial for X motion, ninth-degree polynomial for Z motion,  
506 fourth-degree polynomial for vehicle angle. Different orders were used for respective best matching  
507 of the fitting curve) were applied to fit the time history curves to ensure a smooth MB vehicle  
508 movement. Take Test 01 for instance, the motion of the tracking points corresponding the fitting  
509 curves are shown in Figure B2 (a), (c) and (e). It should be noted since the changes in the Z direction  
510 and theta (vehicle angle) are very small, a minor difference can result in relatively big errors when  
511 tracking the points P1 and P2. To reduce the error, the movements were tracked three times and

512 averaged for each test, see Figure B2 (b), (d) and (f).

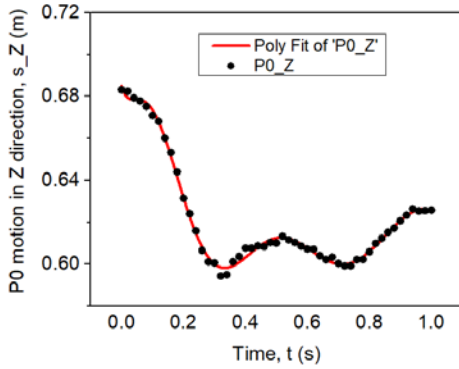
513



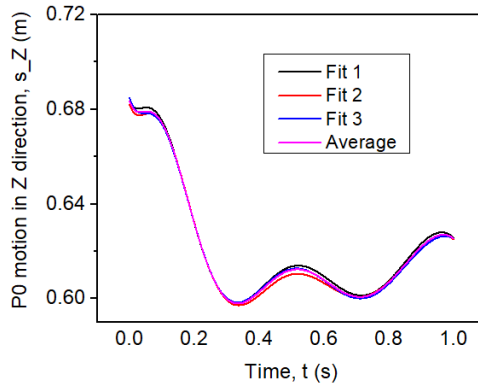
(a) Vehicle X motion



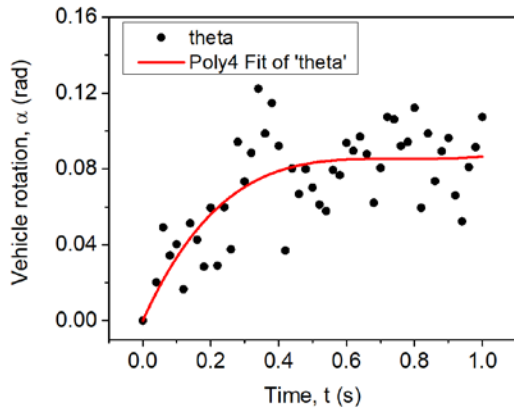
(b) 3 fitting curves of P0 X motion as well as the average curve



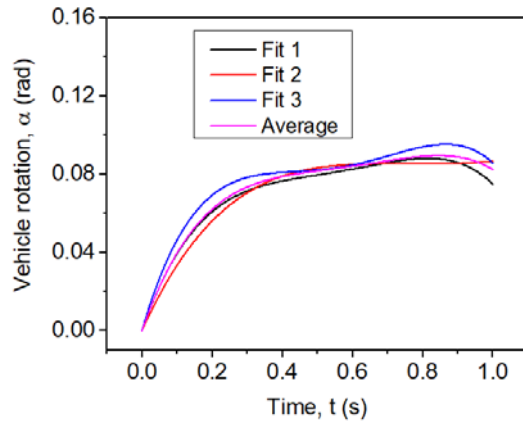
(c) Vehicle Z motion



(d) 3 fitting curves of P0 Z motion as well as the average curve



(e) Vehicle angle



(f) 3 fitting curves of vehicle angle as well as the average curve

Figure B2: The fitting curves of the motion of the tracking point

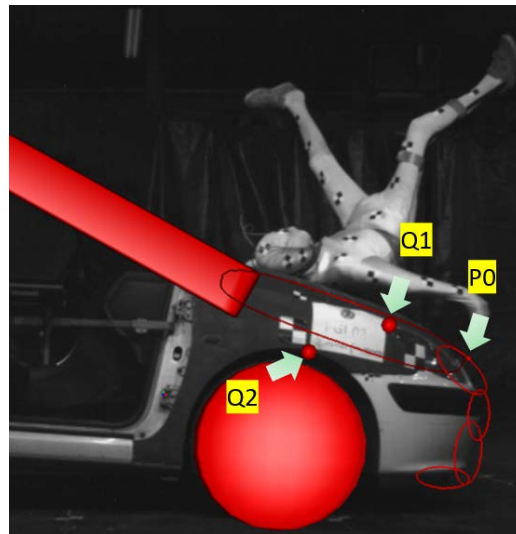
514

515 The input and output motions of the tracking point P0, as well as two other checking points Q1 and

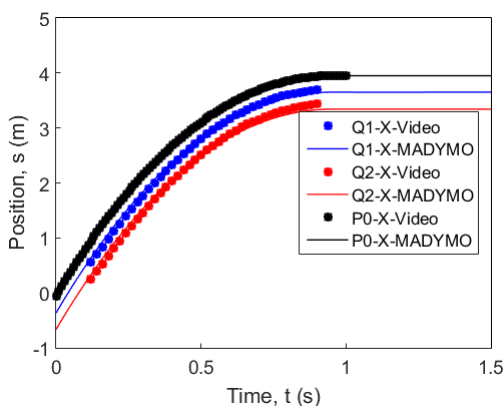
516 Q2 [as demonstrated in Figure B3(a)], were compared to check whether the MB vehicle model

517 moves as well as the input motions. Figure B3 (b) and (c) show that the movement of the tracking  
 518 point P0 and the input is identical. For the two other reference points, the horizontal motion obtained  
 519 from the video of the test and motion obtained from the MADYMO simulation output is closely  
 520 related. The differences in vertical direction were small (up to 3 cm) and may be due to the vehicle's  
 521 rotation angle, which can be ignored. The checking point results indicate the feasibility of using the  
 522 tracking system to capture the vehicle movement.

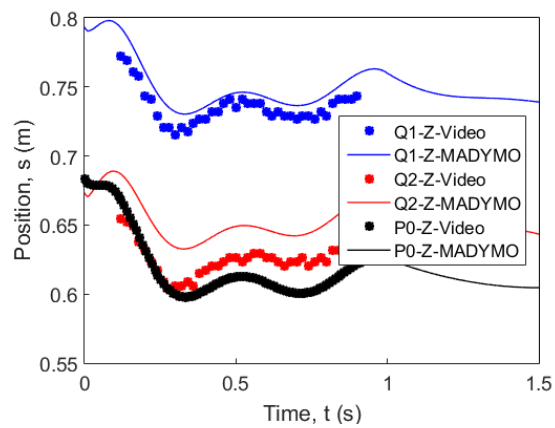
523



(a) The locations of two checking points



(b) X motion



(c) Z motion

Figure B3 The comparison of input and output motions of checking points

524